Cui et al. Nanoscale Research Letters (2015) 10:431
DOI 10.1186/s11671-015-1125-7

Nanoscale Research Letters
a SpringerOpen Journal

NANO REVIEW Open Access

Synthesis and Functions of Ag_2S Nanostructures

Chunyan Cui, Xiaoru Li*, Jixian Liu, Yongchao Hou, Yuqing Zhao and Guocheng Zhong

Abstract

The paper presents a review about synthesis and applications of Ag_2S nanostructures. As the modern photoelectric and biological materials, Ag_2S nanomaterials are potentially useful for both structure and function purposes. Ag_2S is a direction narrow band gap semiconductor with special properties. Ag_2S nanostructures have been widely researched in chemistry and biochemistry fields because of their unusual optical, electrical, and mechanical properties. It can also be used in many fields, such as photovoltaic cells and infrared detector. In the past few years, Ag_2S nanostructures have been synthesized by various methods. The article mainly discusses the four types of preparation methods. Moreover, this article shows a detailed review on the new properties, fabrication, and applications of Ag_2S nanocrystals.

Keywords: Ag_2S nanostructure, Synthesis, Properties, Application

Review

Introduction

Nanoparticles are different from molecular and block materials and have many special physical and chemical properties. In the past decades, the synthetic methods and tuning morphologies of single-component nanocrystalline have made great progress. The metal sulfide nanomaterials have attracted widespread attention due to their suitable band gap, easy manufacturing, low cost, and high performance [1–4].

As an important metal sulfide, Ag_2S is a direction narrow band gap semiconductor (~1.5 eV), and high-absorption coefficient is approximately 10^4 m^{-1} [5, 6]. It also has good chemical stability and optical properties [7, 8], so it is widely used in various fields, such as semiconductor, photovoltaic cells, infrared detector, and superionic conductor [9–12]. Recently, it also has been used in the photoelectric switch and oxygen sensor at room temperature [13]. So far, Ag_2S nanoparticles were successfully prepared by microemulsion method, sol–gel method, particles embedded technology template method, etc. [14–17]. But, it often requires strict preparation conditions, time-consuming, energy consumption, and large size distribution in the traditional production methods. Therefore, simple and economic routes of uniform size distribution of Ag_2S nanomaterials still have challenges.

In this review, we summarized the preparation and properties of Ag_2S materials as follows.

Synthetic Methods

Ag_2S nanostructures have been synthesized by various methods, such as sol–gel method, particles embedded technology template method, etc. Every method has both advantages and limitations. So the preparation methods have still challenges. The new performance of the Ag_2S nanostructures needs to be further exploded. So, the article summarized four types of preparation methods to expect to provide a little help for the workers who are engaging in this field.

Formation of Different Forms of Ag_2S Nanoparticles

Recently, the great efforts have been focused on the morphology control of the semiconductor nanocrystals due to their morphology-dependent properties [18]. Thus, the preparation of different forms of Ag_2S nanoparticles (such as urchin-[19], snow-[20], dendrite-like [21, 22] nanocrystals, and so on) has been caused many scientific research in order to expend their current applications. Various methods in the preparation of Ag_2S nanostructures and their mechanism have been

* Correspondence: lixiaoruqdu@126.com
School of Chemistry Science and Chemical Engineering, Qingdao University, No. 308 Ningxia Road, Qingdao 266071, China

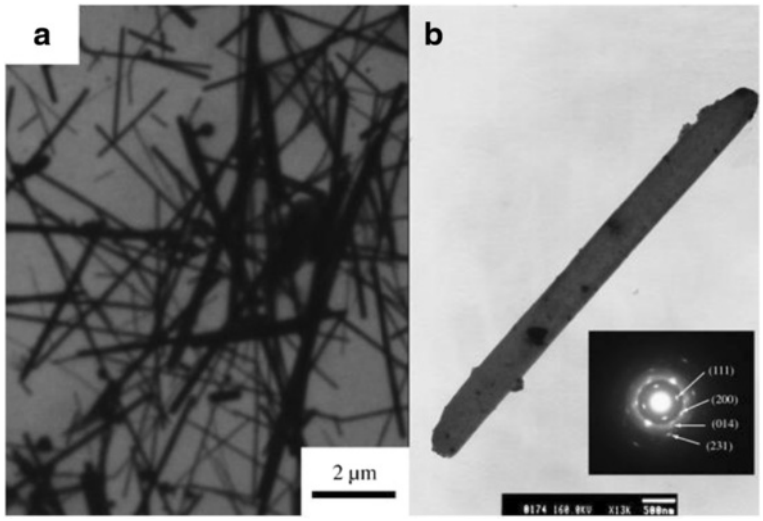

Fig. 1 **a** TEM image, **b** SAED pattern of Ag_2S [23]

explored. For example, Zhao et al. [23] prepared rod-like Ag_2S nanocrystallines by using $Na_2S_2O_3$ as a chalcogen source via gamma ray irradiation at room temperature. In this experiment, polyvinylpyrrolidone (PVP) as a guide reagent of crystal growth plays an important role in the formation of rod-like Ag_2S nanocrystallines. It is well known that high-energy gamma ray irradiation can make H_2O producing strong reductive e_{aq}^- that can initiate many redox reactions to generate ions, which cannot happen in a common atmosphere. And, the homogeneously dispersed $S_2O_3^{2-}$ ions reacted with the generated reductive particles to form S^{2-} [24]. And then, Ag^+ could react with S^{2-} to form Ag_2S nanoparticles. Ag_2S nanorods were formed in the solution of the PVP [25]. Figure 1 shows that the diameters of the nanorods rang from 200 to 500 nm, and the length is up to several ten micrometers. The band gap of Ag_2S nanorods calculated from the UV–vis spectrum is 2.34 eV, which shows an obvious blue shift in UV–vis absorption compared with the bulk Ag_2S (Fig. 2).

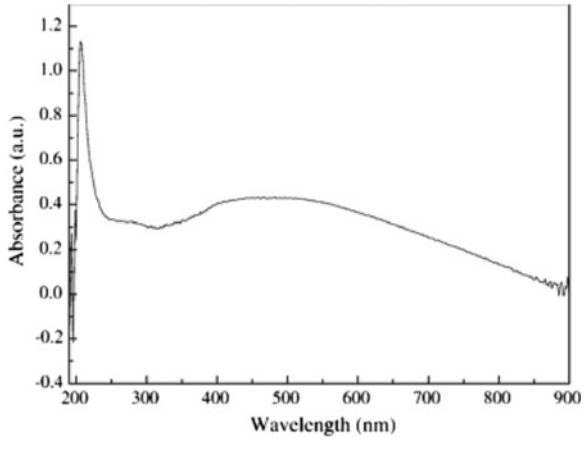

Fig. 2 UV–vis absorption spectrum of as-prepared Ag_2S nanorods [23]

Chen et al. [26] reported that the leaf-like Ag_2S nanosheets were prepared successfully by a facile hydrothermal method in alcohol–water homogenous medium. In the experiment, CS_2 used as sulfur source was dissolved in alcohol and $AgNO_3$ and water at the beginning, respectively. Then the two solutions were mixed together. The reaction is as follows:

$$2NH_3 + CS_2 \rightarrow NH_4NHCSSH \quad (1)$$

$$2Ag(NH_3)^+ + NH_4NHCSSH \rightarrow Ag_2S\downarrow + NH_4SCN + 2NH_4^+ \quad (2)$$

The picture of TEM (Fig. 3) shows all of the samples are leaf-like.

However, Xu et al. [27] reported that the Ag_2S was prepared with an alcohol solution method using CS_2 as sulfur source also. But, all the products were irregular nanoparticles. The reaction medium was changed from water and alcohol–water to alcohol. So, the morphology changed from big irregular nanosheets and microspheres, leaf-like nanosheets nanoparticles to big microspheres, respectively. It is found that alcohol–water homogenous condition and sulfur source of NH_3-CS_2 played the key roles in constructing this unique morphology. That is because the formation of nucleation and growth is expected to be strongly dependent on the properties of the solvent during processes such as coarsening and aggregation [28, 29]. The different morphologies of

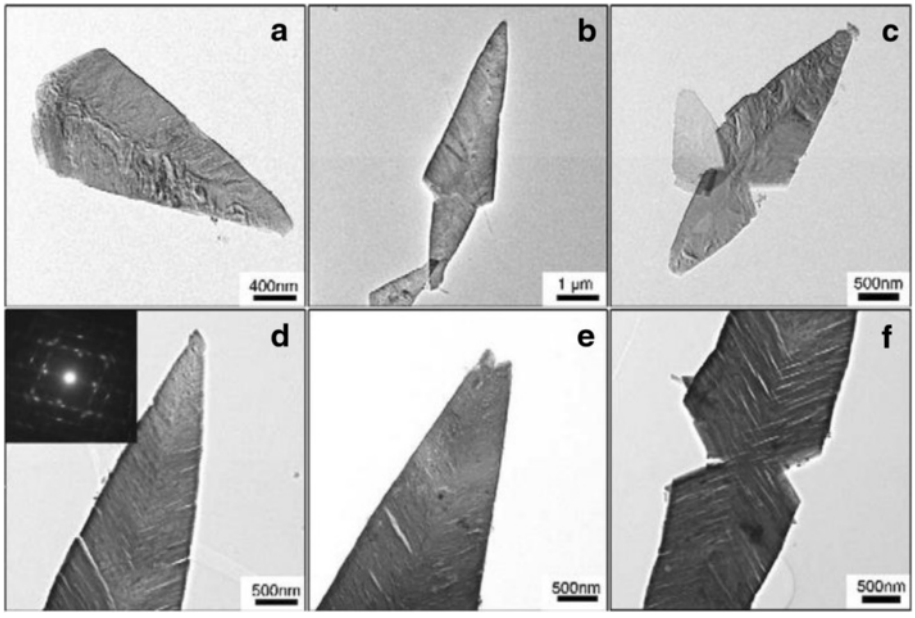

Fig 3 The typical leaf-like morphology TEM image of Ag_2S nanosheets with different magnification, angle and part prepared in alcohol-water medium by hydrothermal treatment at 160 °C for 10h, the insert in (**d**) shows the SAED spots [26]

Ag_2S nano- and micromaterials, including spokewise micrometer bars, nanowires, and nanopolyhedrons have been gained by a facile one-step method at room temperature [30]. In the route, organic template materials were not added into the reaction container. It only changed the ratios of Ag^+, S^{2-}, and ammonia, which may produce the different size and morphologies of the products. In this route, the spokewise microbars of Ag_2S were successfully prepared. Firstly, 10 mL of 0.2 M Tu ($(NH_2)_2CS$) was added in 10 mL of 0.7 % ammonia. Then, 5 mL of 0.3 M Ag_2NO_3 was quickly added in the solution with stirring for 20 min. Last, the product was purified and redispersed in the water several times by centrifugation and sonication (Fig. 4). The methods with other morphologies of Ag_2S were similar to the above process, except for the concentration of ammonia, $AgNO_3$, or Tu. By controlling the concentration of ammonia, $AgNO_3$, or Tu, the morphology of Ag_2S could be easily tuned (Table 1 and Figs. 5, 6, and 7).

Recently, polyhedral nanocrystals including nanocubes have been attracted intensive attention and a variety of face-centered cubicin organic nanocrystals [31–33] have been successfully fabricated. The Ag_2S nanocrystals were also prepared by Lim et al. [34] and Wang et al. [35] by decomposing exothermically organometallic precursor silver thiobenzoate (Ag(SCOPh)) and $Ag[S_2P(OR)_2]$ ($R = C_nH_{2n+1}$), respectively. However, the method often suffers from elaborate

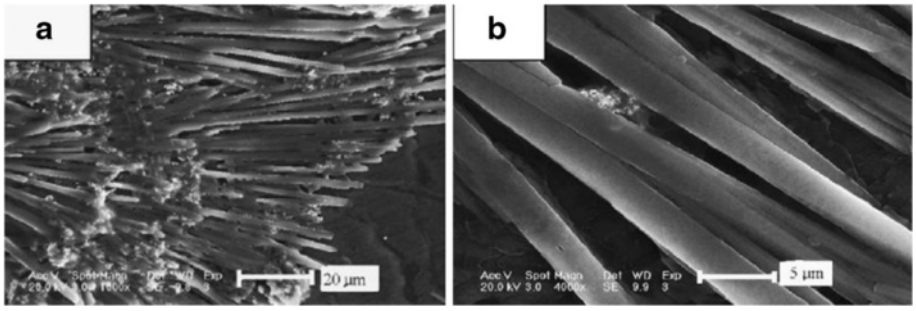

Fig. 4 a FE-SEM image of spokewise microbars of Ag_2S, *scale bar*: 20 μm, mole ratio of Ag^+/Tu: 3/4; **b** Magnified SEM image of the products *scale bar*: 5 μm [30]

Table 1 Starting chemicals used in the syntheses of Ag2S and the morphologies of the products [30]

No.	Concentration of reactants	Quantity of reactants (mL)	Morphologies of products
1	Ammonia 0.7 %	10	Spokewise micrometer bars
	$AgNO_3$ 0.3 M	5	
	Tu 0.2 M	10	
2	Ammonia 0.7 %	2	Microfibers
	$AgNO_3$ 0.06 M	2.5	
	Tu 0.04 M	25	
3	Ammonia 0.7 %	2	Nanowires
	$AgNO_3$ 0.06 M	25	
	Tu 0.04 M	12.5	
4	Ammonia 0.7 %	1	Worn-like nanoparticles
	$AgNO_3$ 0.3 M	5	
	Tu 0.2 M	10	
5	Without ammonia		Nanopolyhedrons
	$AgNO_3$ 0.3 M	5	
	Tu 0.2 M	10	

preparation of air sensitive, expensive organometallic complexes that unstable in air. However, the temperature was high during the experimental with the inert gases protecting. And, the solvent was needed to coordinate. The above method has been improved by Dong et al. [36]. A simple hydrothermal route was reported by modulating the ratio of Tu and $AgNO_3$ with assistance of cetyltrimethyl ammonium bromide (CTAB), respectively. It was also found that the cooperation effect of CTAB and Tu should be responsible for the formation of the as-obtained Ag_2S nanocrystals. Face-centered cubic Ag_2S nanocrystals were synthesized successfully in aqueous medium, which makes the synthesis environmentally benign, user-friendly, economical, and practicable to industry production. The images of SEM showed that the size of the particles ranged from 40 to 80 nm, and the particles with a size of over 100 nm were found occasionally. The typical TEM image showed that most of the Ag_2S nanocrystals particles appeared hexagonal in shape confirming the faceted nature of the nanocrystal. The UV–vis absorption spectrum of the products showed obvious blue shift owe to the small size.

Ag_2S nanomaterials were synthesized by a large number of methods. For example, single-crystalline Ag_2S hollow nanohexagons with better quality and narrower size distribution were successfully reported in aqueous solution at low temperature [37]. The formation mechanism of Ag2S hollow nanohexagons is shown in Fig. 8. Figure 9 displays the SEM images of a typical of Ag_2S nanohexagons. It indicates that the products are good uniformity. In addition, they are hexagonal in shape with a narrower plane size distribution. And, an edge-to-edge distance of 48.9 ± 1.83 nm was achieved by using this approach. From high-magnification TEM image and high-magnification SEM image show that some of these nanohexagons broke. It is shown that they are hollow inside and single crystalline. Because of the high uniformity and Vander Waals interactions, the hollow nanohexagons spontaneously assemble into high-quality ordered arrays [38, 39]. Due to the character, the hollow nanohexagons may have potential applications in fabricating new useful nanodevices in the future. Meanwhile, Rajib Ghosh Chaudhuri et al. [40] reported an easy and novel route for the synthesis of hollow Ag_2S particles by a sacrificial core method in surfactant containing aqueous media. High-aspect-ratio of worm-like Ag_2S nanocrystal with length up to several micrometers and the diameter of 25~50 nm has been successfully prepared by a Triton X-100/cyclohexane/hexanol/water W/O reverse microemulsion in the presence of TAA (thioacetamide) as a sulfur source

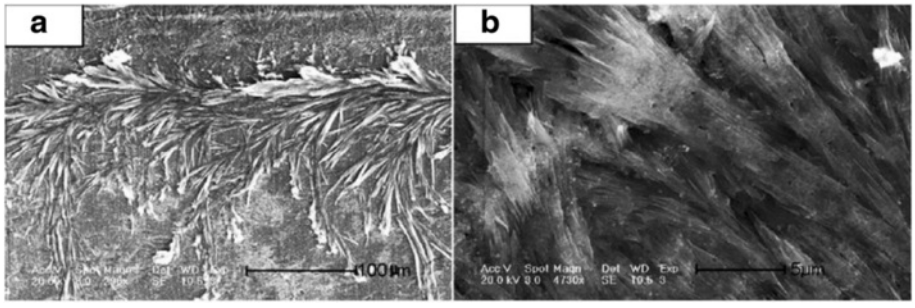

Fig. 5 a FE-SEM image of microfiber like Ag_2S, *scale bar*: 100 μm, mole ratio of Ag^+/Tu: 3/20; **b** Magnified SEM image of the products, *scale bar*: 5 μm [30]

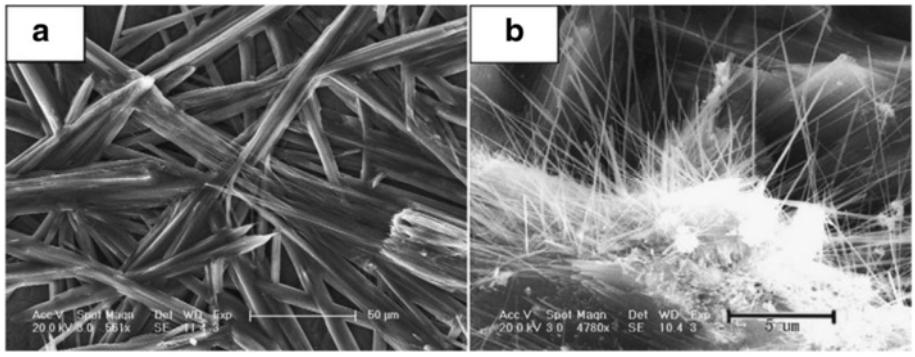

Fig. 6 a FE-SEM image of the aggregated microwires of Ag_2S, *scale bar*: 50 μm, mole ratio of Ag^+/Tu: 3/1; **b** SEM image of Ag_2S nanowires, *scale bar*: 5 μm [30]

and EDTA (ethylenediaminetetraacetic acid) as a chelating ligand [41]. The as-synthesized Ag_2S nanocrystals exhibit strong absorption in UV region, and the absorption edge at about 290 nm (Fig. 10) corresponding to the band gap of 4.3 eV. Compared to the absorption band of bulk Ag_2S (1240 nm, Eg = 1.0 eV) [42], the observed absorption edge is a significant blue-shift. The result is due to the position-dependent quantum-size effect and shape effect. Figures 11, 12, and 13 show the TEM images of Ag_2S nanocrystal synthesized with the typical experimental procedure, in which change one condition. The results indicate that the morphology and size of Ag_2S nanocrystal can be readily controlled by modulating the mole ratio of Ag^+ to EDTA, the molar ratio of water to surfactant (ω_0), and the aging time. The diameter distribution of Ag_2S nanocrystal becomes wider with the increasing ω_0. It can be explanted that at low ω_0 water inside the reverse micelles is considered to be "bound". Therefore, insufficiently available to dissolve the surfactant head group and counterion, the microemulsion becomes more fluid with increasing ω_0, which accelerated the growth of nanocrystalline Ag_2S. The effect of EDTA concentration on the formation of worm-like Ag_2S nanocrystals is important. It can coordinate Ag^+ to form relative stable Ag-EDTA complex, which lowers the effective concentration of Ag^+; TAA could release S^{2-} very slowly in the solution. The two aspects make the $Ag^+$and S^{2-}react slowly, which could result in the separation of nucleation and growth step and is favorable for the directional growth of the crystal nuclei [43]. Ag_2S nanorice was synthesized by reaction between $[Ag(NH_3)_2]^+$ and $Na_2S{\cdot}9H_2O$ in the presence of PVP through hydrothermal method [44]. And, the feature of the Ag_2S nanostructure depends mainly on the type of sliver source, influence of the pyrrolidone rings of PVP, reaction time, and temperature. TEM technique was employed to inspect the morphological variation of the Ag_2S nanoparticles obtained by using different sliver sources (Fig. 14 a and b) at 160 °C for 10 h. It was found that the well-dispersed Ag_2S nanoparticles presented an approximately uniformed rice-shaped morphology. But when $AgNO_3$ was changed into $Ag[(NH_3)_2]^+$ as the sliver source without a control

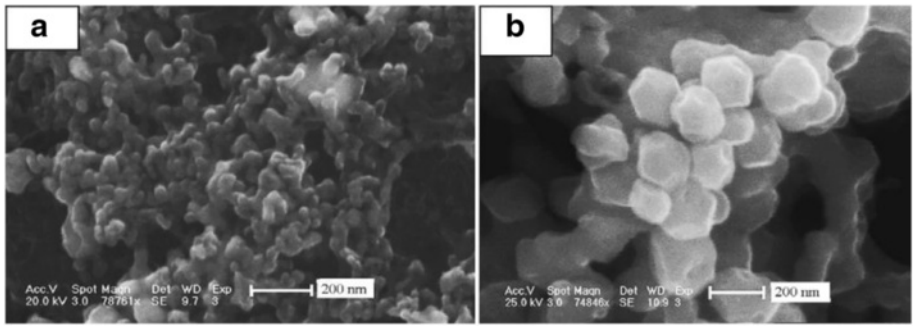

Fig. 7 FE-SEM images of Ag_2S, mole ratio of Ag^+/Tu: 3/4. **a** worm-like nanoparticles, the initial concentration of ammonia: 7 %; **b** Nanopolyhedrons without ammonia [30]

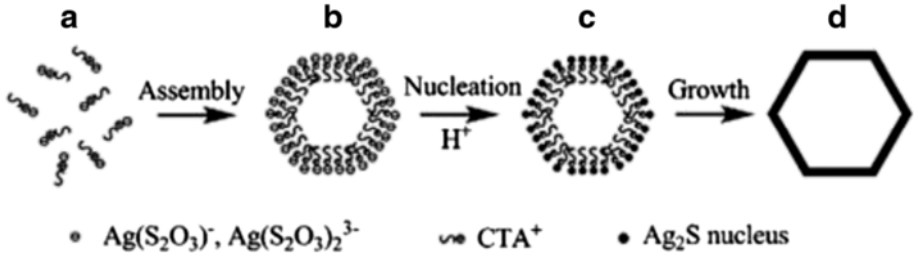

Fig. 8 Schematic representation of the formation mechanism of hollow nanohexagons: (**a**) the soluble CTA^+- $Ag(S_2O_3)$ and CTA^+-$[Ag(S_2O_3)_2]^{3-}$ ion pairs, (**b**) hexagon-like micellar composites with $Ag(S_2O_3)^-$ and $[Ag(S_2O_3)_2]^{3-}$, (**c**) Ag_2S nuclei, (**d**) hollow nanohexagon of Ag_2S [37]

over the Ag^+ release rate provided by ammonia complexation during the reaction, the rice-shaped morphological feature of Ag_2S nanoparticles would not been seen, and anamorphous appearance would be presented instead. So, Ag^+ concentration had a key impact over the formation of the Ag_2S nanorice. Similar condition also happened while reaction time influences on the experimental results (Fig. 14 c and d). It can be explained by the famous Ostwald ripening mechanism. The FI-IR spectra of pure PVP, Ag_2S nanorice-associated PVP are shown in Fig. 15. It is easy to find that the pyrrolidone ring plays an important role in the formation of the Ag_2S nanorice. Normal and flattened rhombic dodecahedral submicrometer Ag_2S particles were prepared by adjusting the ratio of Tu to $AgNO_3$ and volume of concentrated HCl aqueous solution [45].

Preparation by Using Bionic Technology

In recent years, the synthesis of quantum dots (QDs) with biological macromolecules route has attached great attention [46]. In previous works, CdTe QDs with good biocompatibility by using RNase A as the template was synthesized successfully [48]. But, it is not popular

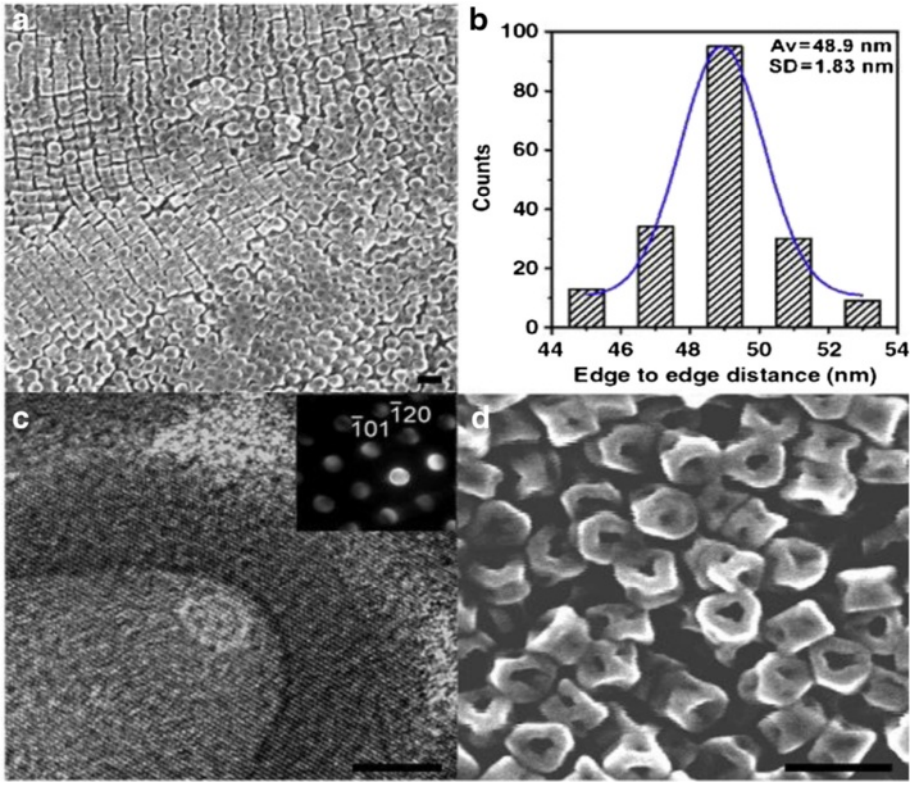

Fig. 9 **a** Low-magnification SEM image of hollow nanohexagons, **b** Plane size distribution of hollow nanohexagons, **c** High-magnification TEM image of hollow nanohexagons, and **d** High-magnification SEM image of hollow nanohexagons. The *inset* is the corresponding electronic diffraction pattern from one nanohexagon. *Scale bars*, **a** 100 nm, **b** 5 nm, and **c** 100 nm [37]

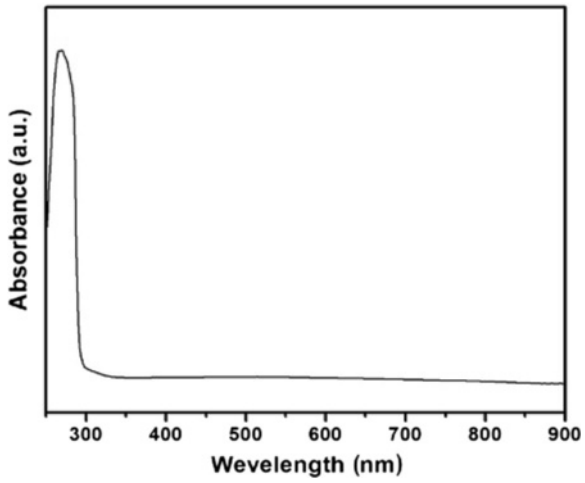

Fig. 10 UV–vis absorption spectra of Ag_2S nanocrystal synthesized in W/O microemulsion ([TAA] = 0.3 mol/L, $[Ag^+]$ = 0.1 mol/L, $[Ag^+]$/[EDTA] = 1) aged for 3d with $\omega_0 = 10$ [41]

enough because of the toxic nature of Cd and Te. Ag_2S QDs is treated as an ideal optical probe because it has lower toxicity compared with previous prepared near-infrared (NIR) QDs which was synthesized in organic phase. But, the process may cause extra environment pollution [49, 50]. The synthesis of QDs with fluorescence emission from UV to NIR regions has made great progresses as optical probes for in vitro and in vivo molecular imaging [47]. So, the highly monodisperse and water soluble RNase-Acopped-Ag_2S QDs clusters were synthesized via biomimetic route in aqueous phase [51]. The QDs have low cytotoxicity and good biocompatibility. Meanwhile, the produce process is environmental friendly. From the images (Fig. 16), it indicates that RNase A-Ag_2S QDs clusters with irregular morphologies were dispersed, and the Ag_2S nanocrystals have clear lattice fringes. Furthermore, X-ray diffraction (XRD) image shows that the prepared Ag_2S QDs assumed the crystalline structure of monoclinic α-Ag_2S. Tetrazolium-based colorimetric assay (M77 test) shows that RNase A dose not only serves as a stabilizer agent in the formation of Ag_2S QDs to avoid aggregation but also is a biomolecule to modify the surface of Ag_2S QDs to decrease toxicity. So, the products have great potential application in molecular imaging in living cells and tissues. Biomolecules assisted the formation of inorganic nanostructures, facilitate the electrostatic stabilization, and thus improving optical properties.

Siva C et al. [52] reported that Ag_2S nanostructure was obtained using Ag^0 nuclei as a core. Biomolecule (L-cysteine) can act as a sulfur source and stabilizing agent which prevents the agglomeration [53]. Meanwhile, they also have obtained the novel Ag_3AuS_2 nanocrystals by adopting the gold ions in the L-cysteine-assisted Ag_2S formation. The FT-IR images (Fig. 17) show that one L-cysteine molecule is interconnected to another via hydrogen bonding. From Fig. 18, it is clear that the Ag_2S nanocrystals are almost uniform in their size and are interconnected among themselves, and their average particle size is 5.2 nm. Meanwhile, the Ag_3AuS_2 nanocrystals are also connected with themselves. The Ag_3AuS_2 nanocrystals are non-uniform in their sizes, and the average size is 9.1 nm. Self-organized nanocrystal architectures with subnanometric spatial resolution also obtained by mimicking the biological crystal growth [54].

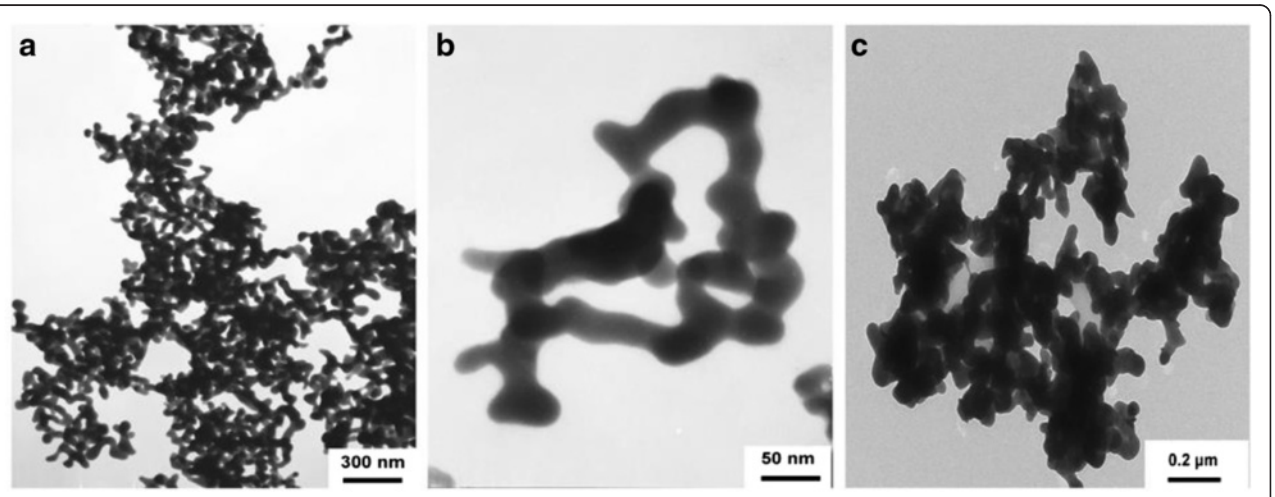

Fig. 11 TEM images of Ag_2S nanocrystal synthesized in W/O microemulsion ([TAA] = 0.3 mol/L, $[Ag^+]$ = 0.1 mol/L, $[Ag^+]$/[EDTA] = 1) **a**,**b** aged for 3d, **c** aged for 24d with $\omega_0 = 10$ [41]

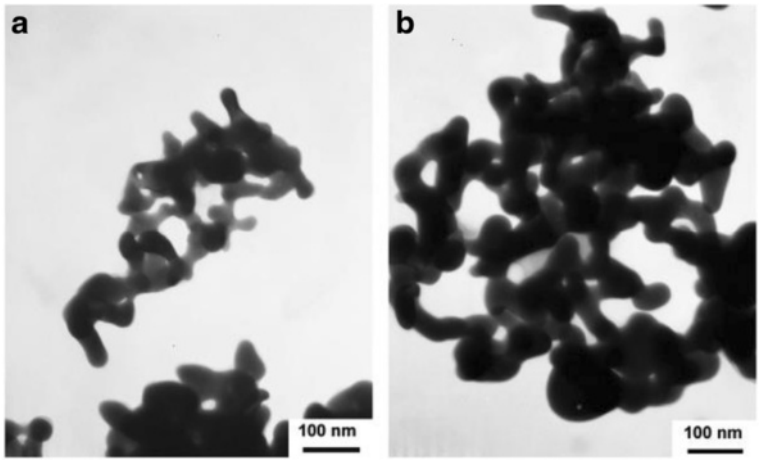

Fig. 12 TEM images of Ag_2S nanocrystal synthesized in W/O microemulsion ([TAA] = 0.3 mol/L, $[Ag^+]$ = 0.1 mol/L, $[Ag^+]$/[EDTA] = 1) aged for 3d with **a** $\omega_0 = 6$, **b** $\omega_0 = 15$ [41]

Preparation by a Single Molecular Precursor of Decomposition

Among the many methods for synthesizing metal chalcogenide materials, the single molecular precursor route has some appealing features [55, 56]. On the one hand, it offers the distinct advantages of mildness, simplicity, safety, and particular compatibility with the metalorganic chemical vapor deposition [57]. On the other hand, the molecular precursor may be related to the unusual crystal growth selectivity or metastable phase formation of the resultant products, which are sometimes unattainable via conventional synthesis techniques [55, 56]. For example, Ag_2S nanocrystals were achieved via a modified hot-injection process from a single-source precursor molecule Ag(SCOph). When the precursor molecule is injected into a preheated reaction system at 160 °C, spherical Ag_2S nanocrystals are directly obtained [58]. Wang et al. [59] obtained the Ag_2S crystallites by heating the Ag-DDTA in air at 200 °C for 3 h and used an air-stable single-source molecular precursor (Ag-DDTA) as the react source. The method is both economic and non-toxic. Monodispersed and size-controlled Ag_2S nanoparticles were synthesized successfully via a green and simple surfactant-free solventless thermolysis of silver xanthates as single-source precursors [60]. In the experiment, the diameter of Ag_2S nanoparticles is from 8.9 ± 1.2 nm to 48.3 ± 3.6 nm (Fig. 19). And, the "Size control" was

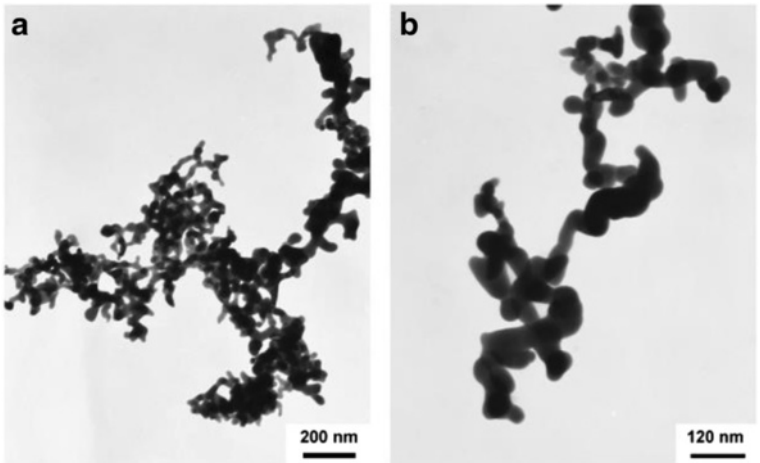

Fig. 13 TEM images of Ag_2S nanocrystal synthesized in W/O microemulsion ([TAA] = 0.3 mol/L, $[Ag^+]$ = 0.1 mol/L) with various concentrations of EDTA **a** $[Ag^+]$/[EDTA] = 2, **b** $[Ag^+]$/[EDTA] = 4 aged for 3d with $\omega_0 = 10$ [41]

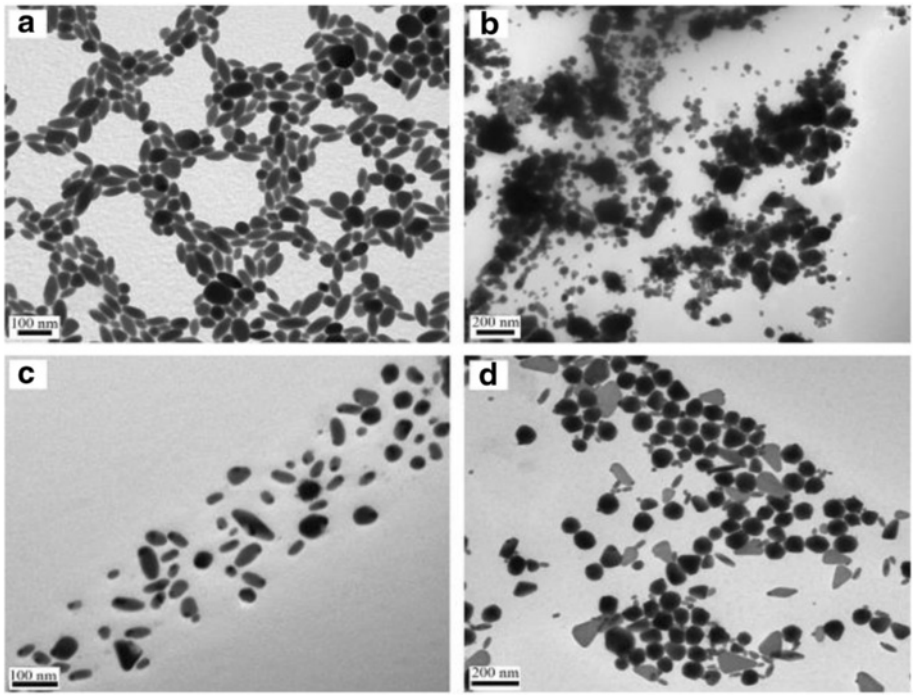

Fig. 14 TEM image of Ag_2S nanoparticles synthesized under different experimental conditions: **a** typical experiment, **b** using $AgNO_3$ as the silver source, **c** 160 °C, 4 h, and **d** 160 °C, 13 h[44]

achieved by simply changing the alkyl chain length in the precursor. The grain size of Ag_2S nanoparticles decreases with the increase of the alkyl chain length of the precursors. At the same time, with the temperature increasing, the xanthate ligand will be absorbed onto the surface of Ag_2S nanoparticles to control particle growth. Figure 20 shows the possible growth mechanism.

Other Methods of Preparation

In addition, there are many other methods. For example, Ag_2S nanocrystals were prepared via a facile solution growth method, in which Ag_2S and sulfur powder are used as precursors. Oleylamine is used and act as both reducing agent and stabilizer during the synthetic process [61]. The obtained Ag_2S nanocrystals can be used as substrates for surface-enhanced Raman scattering (SERS) detection in this method. SERS spectra of rhodamine 6G can be detected, the synthesis strategy is simple, and the obtained samples have great potential for high sensitive optical detection. This character may attract much interest in fundamental physics as well as device application points of view. Maryam Shakouri-Arani et al. [62] have produced the Ag_2S nanoparticles by a solvothermal process; a new sulfuring agent from class of thio Schiff-base benzenethiol was used in the presence of various solvents. In this paper, we also found that the shape and size of the Ag_2S can be controlled by means of setting certain reaction parameters such as the reaction temperature, presence of surfactant, and type of solvent (Fig. 21).

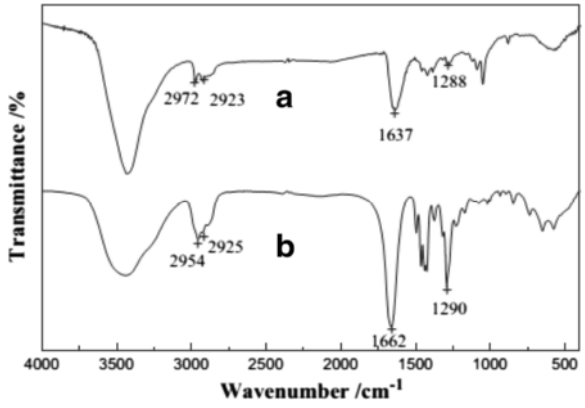

Fig. 15 a FT-IR spectra of PVP-AgPVP-Ag_2S, and **b** pure PVP [44]

Performance Study

Application in Biotechnology

In recent years, Ag_2S nanometer materials in the application of biotechnology have gradually aroused people's concern and attention. Many efforts have been devoted to identifying NIR-II emitting agents for in vivo imaging applications. QDs such as PbSe, [63] PbS, [64] and CdHgTe [65], with NIR emission, were successfully

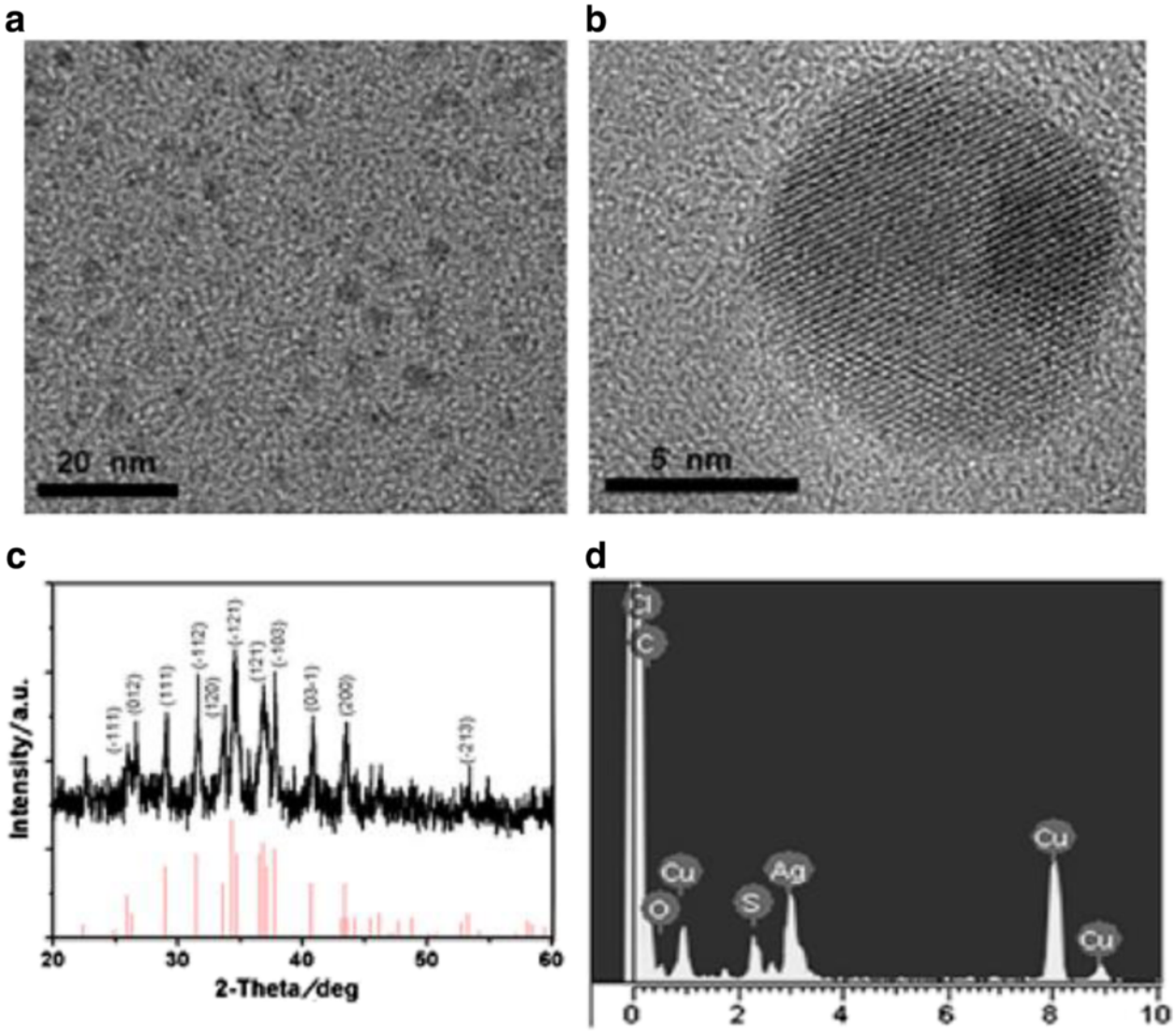

Fig. 16 **a** TEM image of fresh prepared RNase A-Ag_2S QDs. **b** The high-resolution TEM (HR-TEM) image of an individual RNase A-Ag_2S QD. **c** Powder X-ray diffraction (XRD) pattern of RNase A-CdS QDs. **d** EDS spectrum of RNase A-CdS QDs [51]

obtained. But, the highly toxic nature of Pb, Cd, and Hg is of concern for in vivo applications [66]. And, well-designed carbon nanotubes also have been regarded as biological imaging agent in the NIR-II region. However, the disadvantage is the lower fluorescence quantum yield of carbon nanotubes [67, 68]. So, Zhang et al. [69] made a study for Ag_2S QDs, which combined with other biomacromolecules to become the imaging agent. Because Ag_2S QDs should be more biocompatible owning to the absence of any toxic metals such as Cd, Pb, and Hg. And, Ag_2S also exhibits an ultra-low solubility product constant (Ksp $= 6.3 \times 10^{-50}$) which ensures the minimum amount of Ag^+ released into the biological surroundings. Ag_2S QDs have high-emission efficiency in the unique NIR-II imaging window. So, there are a lot of characters such as deep tissue penetration, high sensitivity, and elevated spatial and temporal resolution; the water-soluble Ag_2S QDs terminated with carboxylic acid group were synthesized by one-step method reported [70]. The Ag_2S QDs exhibited bright photoluminescence and excellent photo stabilities. Therefore, the photoluminescence emission could be turned from visible region to near-infrared (NIR) region (from 510 to 1221 nm). So, it has the opportunity to study nanodiagnostics and imaging. In vivo imaging experiment, the Ag_2S QDs were injected into the nude mice subcutaneous tissue or abdominal cavity. As

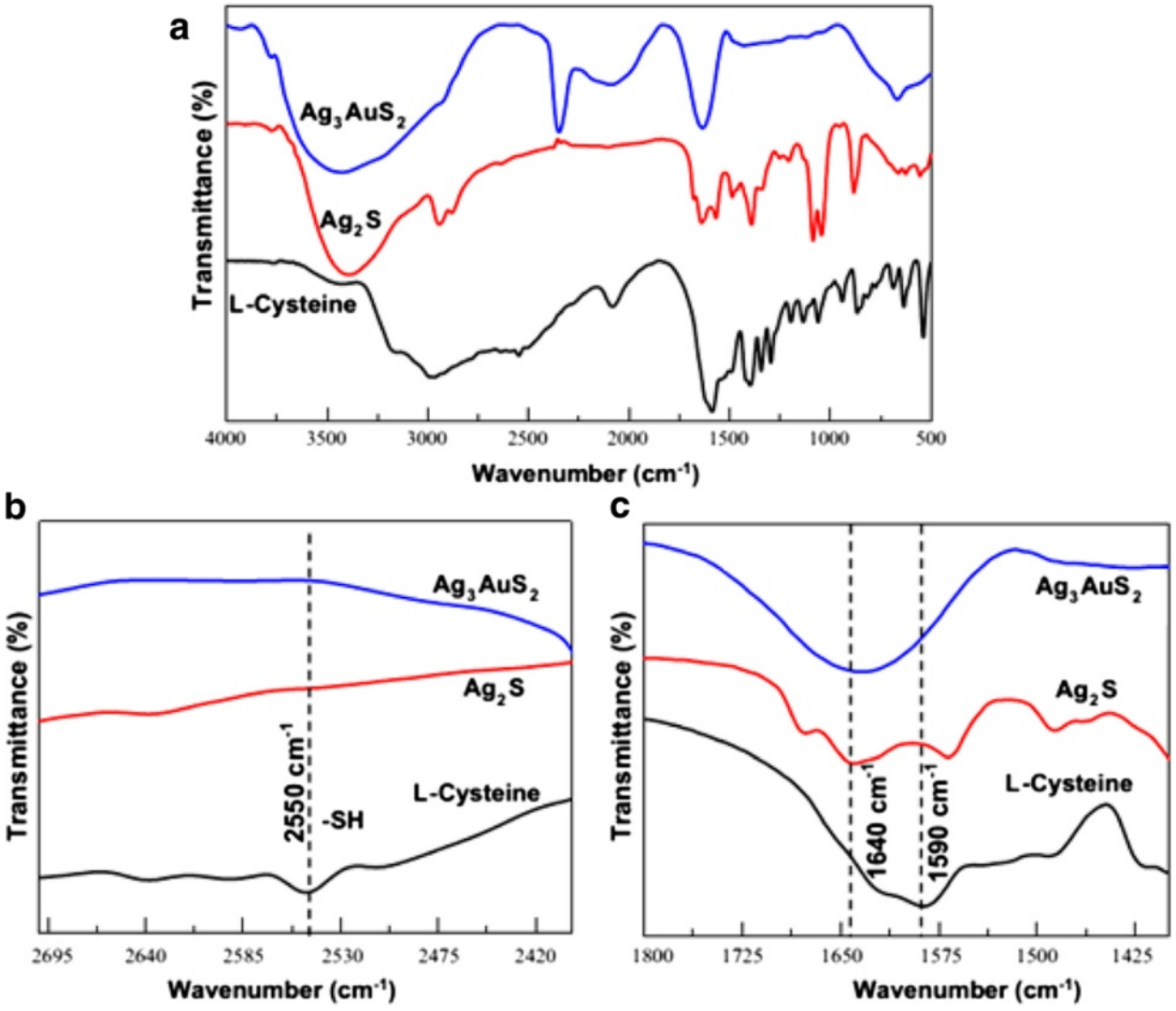

Fig. 17 **a** FT-IR spectrum of L-cysteine, Ag_2S, and Ag_3AuS_2 nanocrystals. **b** and **c** are the magnified graphs to show the-SH stretching, and carboxylic group interaction [52]

shown in Fig. 22a–c, bright spot of Ag_2S QDs fluorescence was observed in the mice with subcutaneous and celiac injection compared with the ordinary mice. From the PL spectra (Fig. 22d), it can be seen that the fluorescence emitted from the injection region differ with the auto fluorescence from the other region of the mice body. It indicated that the fluorescence of the as-prepared Ag_2S QDs can penetrate the body of nude mice. And, the fluorescence emitted from the celiac region was clear and bright. It suggested that the Ag_2S QDs fluorescence was less affected by the body auto fluorescence. At the same time, the Ag_2S QDs do not contain toxic elements to body. Thus, it has great potential in vivo imaging. And then, Ag_2S nanocrystals were applied into DNA hybridization analysis [71]. A DNA probe labeled with Ag_2S nanoparticles, which detection limit can be attained up to picomoles per liter. It indicated that the product have high sensibility and selectivity. Furthermore, this surfactant-capped Ag_2S product is likely to be of potential application value in electrochemical detection and biosensors.

Application in the Catalytic and Decomposition

Nowadays, a shortage of clean water can lead to serious problems and diseases. So, water purification problems become more and more important. But, many textile dyes are difficult to degrade with the common methods due to their synthetic origin and the presence of a complex aromatic structure [72, 73] TiO_2 is often used as

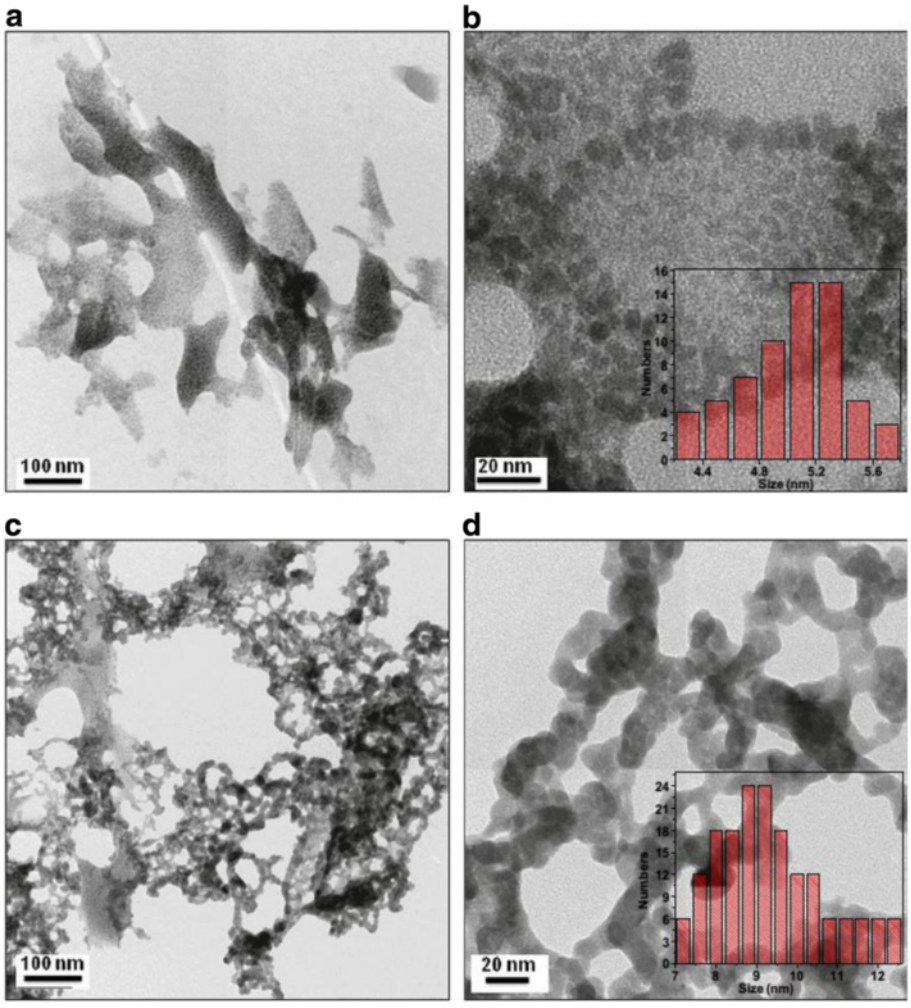

Fig. 18 HRTEM images of Ag_2S (**a**, **b**), Ag_3AuS_2 (**c**), and nanocrystals (**d**). *Insets* are the histogram of particle size distribution [52]

catalytic to remove dyes and phenolics for their higher photocatalytic activity, good photo stability, non-toxicity, and low price. However, the large band gap of TiO_2 (3.2 eV) limits its photocatalytic applications in the UV range and reduces its catalytic efficiency. Because of the unique structure of Ag_2S, it is expected to be the new type catalyst. And because of the unique structure of Ag_2S, it can expect to be the new type catalyst. For example, Ag_2S nanoparticles were prepared by using a hydrothermal method and Ni was doped via a photo-assisted deposition method [74]. The XRD images of the parent Ag_2S and Ni/Ag_2S nanoparticles are contrasted in Fig. 23. They found that the structural characteristics of Ag_2S and Ni/Ag_2S are mainly composed of Ag_2S. It indicated that the Ag_2S structure remained conserved after the application of the photo-assisted deposition methodology. From the UV–vis diffuse reflectance spectra of the Ag_2S and Ni/Ag_2S nanoparticles, they calculated that the energy gap decreased with the increasing Ni ions. Ni used as a trapping site captures photo-generated electrons from the conduction band and separates the photo-generated electron–hole pairs. This change would force Ag_2S to be activated more easily in the visible region, so it can enhance the light absorption ability of the catalysts. And, the catalyst could be reused without any loss in activity for the first 5 cycles. Compared with pure semiconductors, Ag_2S loaded mesoporous materials in general possess greater photocatalytic activity.

The advantages using zeolite or mesoporous support for semiconductor photocatalysis include formation of ultrafine semiconductor particles during sol–gel deposition, increased adsorption in the pores, surface acidity which enhances electron-abstraction, and decreased UV-light scattering as the main component of

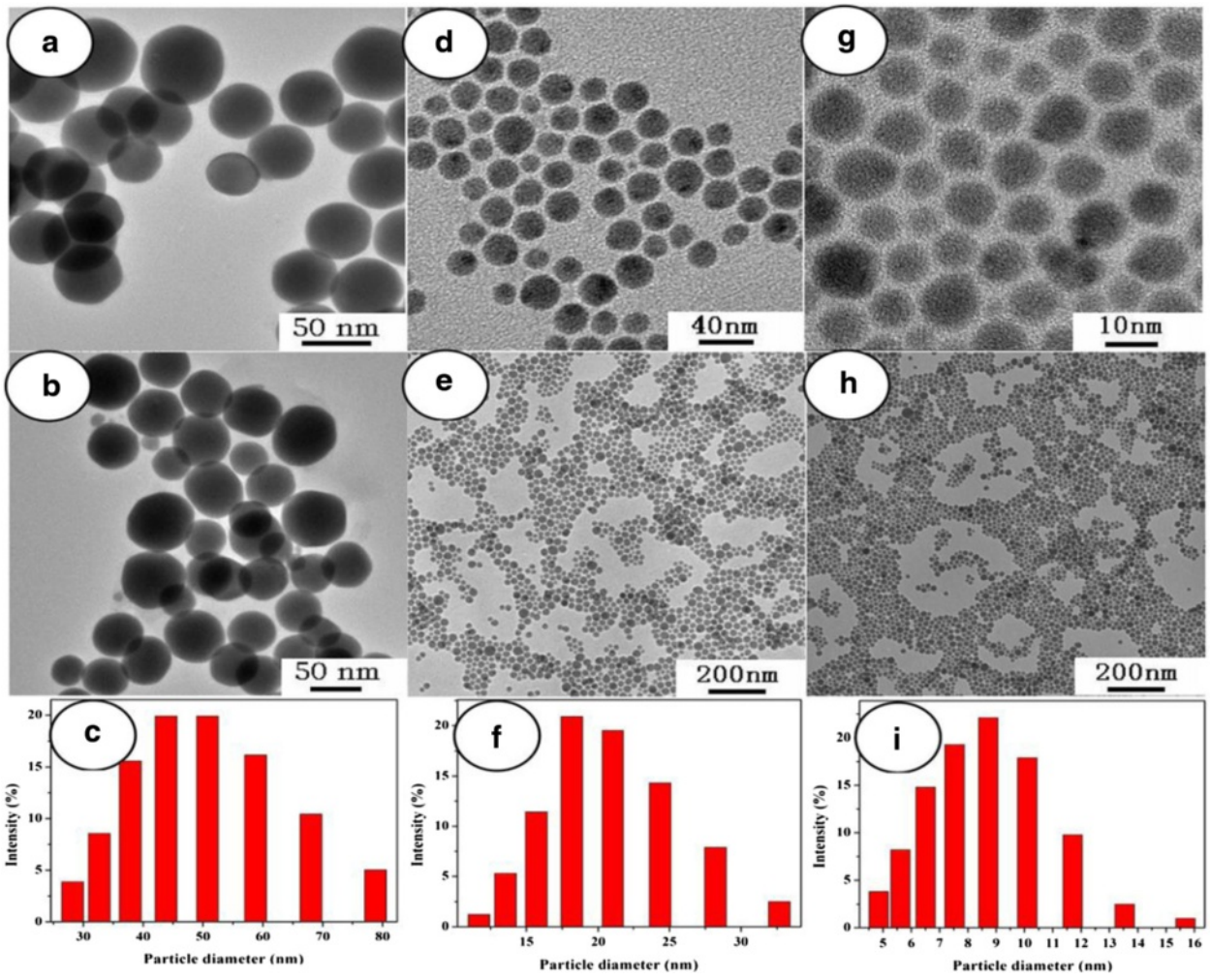

Fig. 19 TEM images and corresponding size distribution of Ag_2S nanoparticles synthesized by solventless thermolysis of silver octyl xanthate (**a**–**c**), silver hexadecyl xanthate (**d**–**f**), and silver carnaubyl xanthate (**g**–**i**) [60]

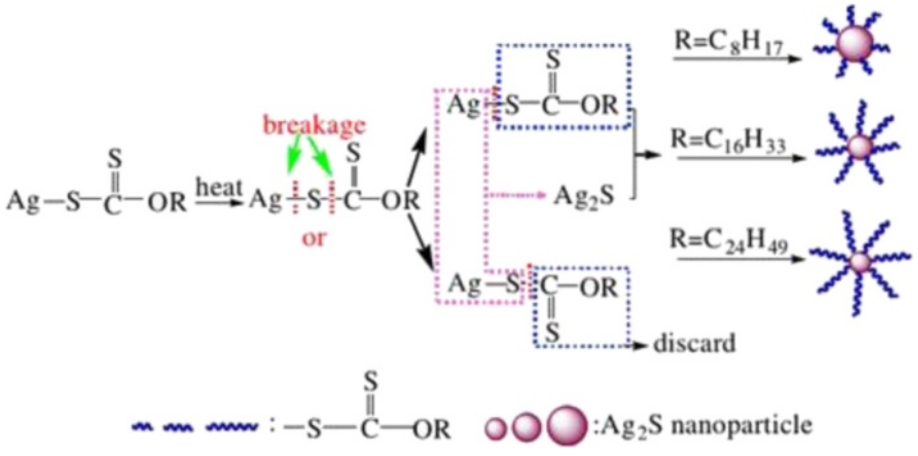

Fig. 20 Schematic diagram of the possible growth mode [60]

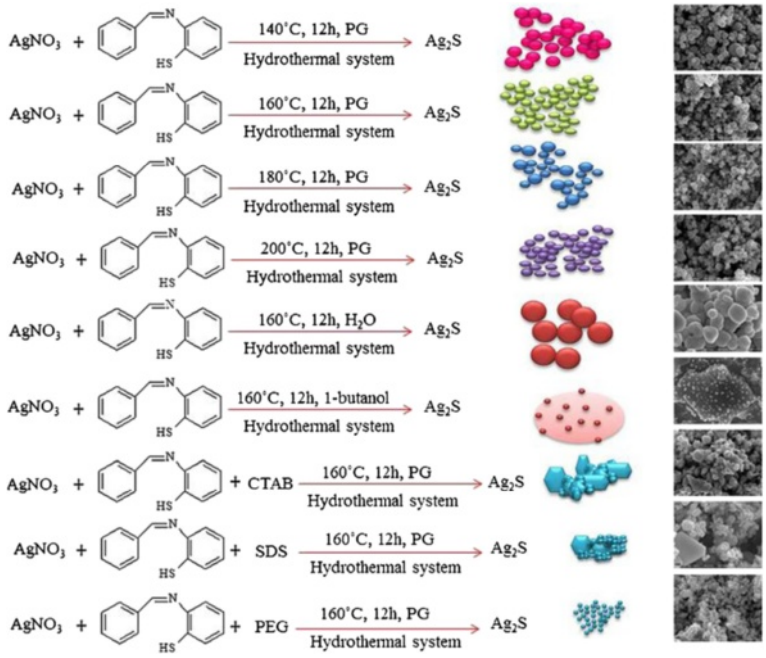

Fig. 21 Schematic diagram illustrating the formation of Ag2S samples at various conditions [62]

zeolite is silica [72, 73]. A. Pourahmad prepared the Ag_2S/MCM-41 photocatalysts by ion exchange method and is used for the photocatalytic degradation of methylene blue [75]. Figure 24 is the time-dependent electronic absorption spectra of dye during photo irradiation. After 20 min of irradiation under UV light in a Ag_2S/MCM-41 suspension, 94 % of dye was decomposed and decolorized. And, no new bands appear in the UV–vis region due to the reaction intermediates formed during the degradation process. Under UV irradiation, Ag_2S, MCM-41, and Ag_2S/MCM-41 materials on photodegradation of methylene blue are shown in Fig. 25. It is observed that Ag_2S supported system has a higher rate of degradation than Ag_2S or MCM-41 alone. And, there are many factors that can influence the efficiency of nanocomposite catalyst, such as the amount of Ag_2S loading, PH, and initial concentration of dye. Several methods have been reported concerning the photosensitization of TiO_2 by M_xS_y or M_xO_y nanoparticles for heterogeneous photocatalysis [76] including CdS [77] or WO_3 [78]. In fact, nanocrystalline Ag_2S is a good candidate for the photosensitization of TiO_2 catalysts, for Ag_2S has a direct band gap of 0.9–1.05 eV, and its conduction band (−0.3 eV) is less anodic than the corresponding TiO_2 band (−0.1 eV), and the valence band (+0.7 eV) is more cathodic than the TiO_2 valence band (+3.1 eV). So, distinct TiO_2/Ag_2S nanocomposites were prepared by a single-source decomposition method [79]. After, the sensitized TiO_2 materials were evaluated as photocatalysts on the degradation of aqueous phenol solutions, and the photocatalytic activity of nanocomposites was enhanced with the existence of Ag_2S over the TiO_2 surface. And, the efficiency of this photocatalysts is considerably improved comparing with pure TiO_2. The best phenol photocatalyst was obtained when atomic ratio of Ti/Ag is 2.40. Nanostructured Ag_2S/CdS was synthesized by two-step precipitation method [80]. And, the composite materials have certain photocatalytic performance. When the concentration of Ag_2S was 5 % by weight, Ag_2S/Cds showed the highest photocatalytic activity for hydrogen evolution, with the solar-hydrogen energy conversion efficiency approximately 0.7 %. So, after doped Ag_2S, the photocatalytic activity of CdS have enhanced obviously.

Application in Optoelectronic Devices

Compared with bulk counterparts, the sheet-like photocatalysts are much better for continuous flow system because of ease separation and recovery from the reaction system [86]. The sheet-like photocatalysts can also help to harvest light more efficiently [87]. So, a novel graphene sheet/Ag_2S composite was synthesized through a facile solvothermal method, and its electrochemical performance was carried on a modified glassy carbon electrode in a three-electrode

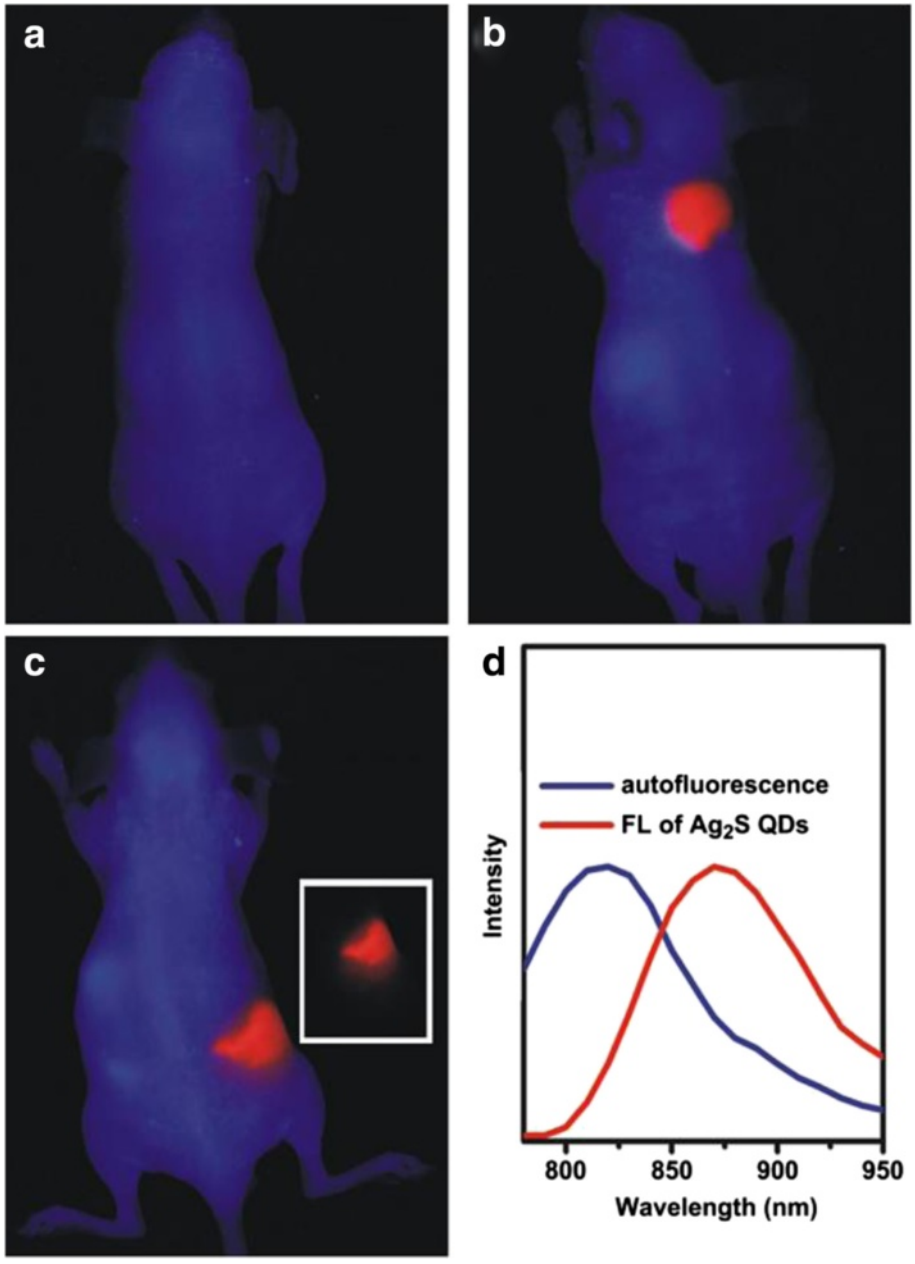

Fig. 22 In vivo NIR fluorescence imaging (pseudocolored image) of nude mice. Control experiment (**a**), with subcutaneous injection (**b**) and with celiac injection (**c**) of Ag_2S quantum dots emitting at 910 nm; Unmixed image of Ag2S quantum dots fluorescence signal (*C inset*); The corresponding emission spectra of the auto fluorescence and QD fluorescence of mice with celiac injection (**d**). (In images **a**–**d**, the *blue* corresponded to the mice auto fluorescence and the *red* corresponded to QD fluorescence.) (For interpretation of the reference to color in this figure legend, the reader is referred to the web version of this article.) [70]

electrochemical cell [81]. In Fig. 26, it can be clearly seen that the pure graphene oxide sheets naturally aggregate and stack to multilayers with numerous edges, and the surface of graphene oxide was very smooth compared with graphene sheets doped with Ag_2S NPs. So, the morphology of G-Ag_2S composites has a substantial difference from that of the Go sheet. Figure 27 shows that the composite modified GCE shows redox peaks, but graphene modified exhibits a perfect rectangle curve, and the redox peaks of the composites, often a characteristic of pseudocapacitance mainly result from the redox transition of Ag_2S between a semiconducting state and a conducting state. And, it is calculated that the redox peaks

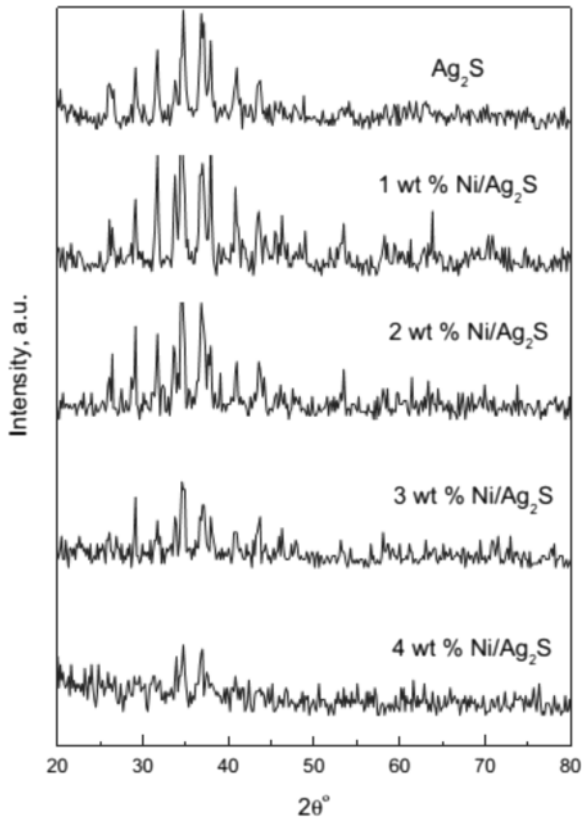

Fig. 23 XRD pattern of Ag_2S and Ni/Ag_2S nanoparticles [74]

with the specific capacitance is 1063 Fg^{-1}, but the specific capacitance of graphene modified is 316 Fg^{-1}. So, it is believed that the nanocomposites would be a promising candidate as supercapacitor materials for practical applications in future electronic devices. At the same time, graphene-like Co_3S_4 nanosheet/Ag_2S nanocomposite was prepared using a simple method. The nanocomposite photocatalyst displays excellent stability and photocatalytic activity compared with pure Co_3S_4 nanosheet or Ag_2S nanoparticles [85]. Ag_2S is an important material for optoelectronic, because it has an energy gap of Eg~1.1 eV, which is similar to the ideal band gap of 1.13 eV for a photovoltaic device [82] indicating that Ag_2S could be an optimal solar absorber performance which was measured to the battery. The Ag_2S QDs were synthesized by the successive ionic layer adsorption and reaction deposition method [83]. And, the assembled Ag_2S-QD solar cell in $\lambda = 530$ nm has the biggest external quantum efficiency (EQE) which was 59 %, and when the spectral range in 400–1000 nm, the average of EQE was 42 %. The effective scope of photovoltaic is full of visible light and near-infrared spectral regions. Therefore, the results indicate that Ag_2S QDs can be used as a highly efficient and broad band sensitizer for solar cells. R. Karimzadeh et al. [84] found that about 3 nm Ag_2S semiconductor nanocrystals in concentrations of dimethyl sulfoxide solution has different non-linear refractive properties; it can be used as a low power optical-limiting device. In addition, Ag_2S also has important application in other areas, for example nanometer-scale non-volatile memory devices. [88].

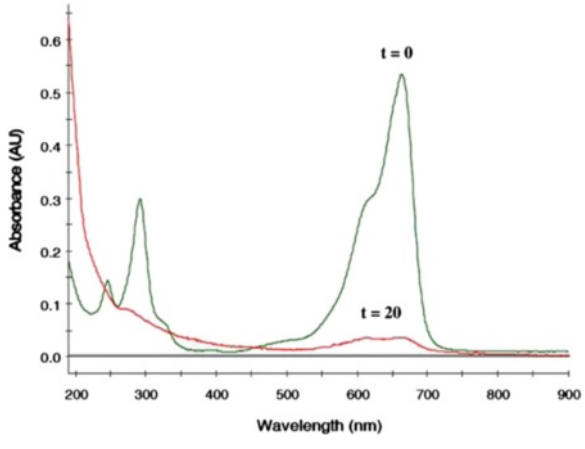

Fig. 24 Spectra change that occur during the photocatalytic of aqueous solution of methylene blue: PH = 7. [20 wt% Ag_2S/MCM = 41] = 0.6 g/L. $C_0 = 0.32$ ppm [75]

Other Applications

Ag_2S nanomaterials also have many other properties in various fields, such as electronic, magnetic, and so on. Ag_2S belongs to I-VI semiconductor materials with monoclinic crystal structure. Thin films of Ag2S have applications in photoconducting cells [89], IR detectors [90], and solar selective coating. Thus, Ag_2S is a promising material for the conversion of solar energy into electricity as its band gap is between 1 and 2 eV. Usually, the material design for these technological applications is based on thin film preparation techniques, in which the film thickness ranges from micrometer to submicrometer. It is well known that the surface contribution to the electric transport process could be evaluated when thin films with different thicknesses, i.e., with various surface-to-volume ratios, are investigated [91]. So, D. Karashanova et al. [92] evaluated the surface contribution to the electronic or ionic transport in the epitaxial silver sulfide films using electron-conducting and electron-blocking contacts, respectively. At the same time, Ag/Ag_2S also can become the electrode materials, but disadvantages of the solid-state Ag/Ag_2S electrode such as non-ideal response, signal drifting, and a long response time at low sulfide levels have

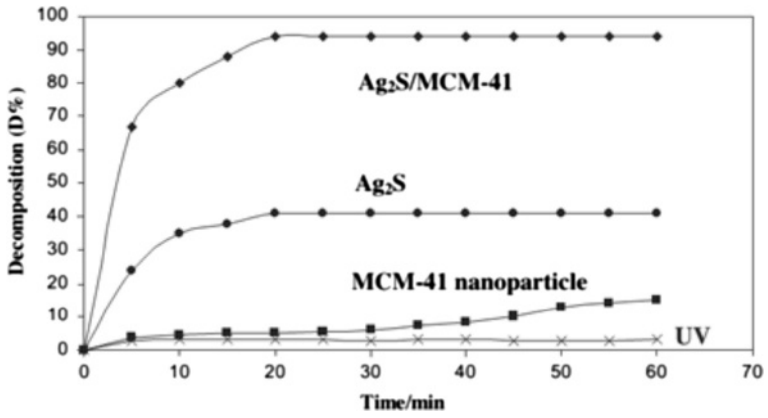

Fig. 25 Effect of UV light and different photocatalysts on photocatalystic degradation of methylene blue. $C_0 = 0.32$ ppm. [20 wt% Ag_2S/MCM-41] = 0.6 g/L, PH = 7 [75]

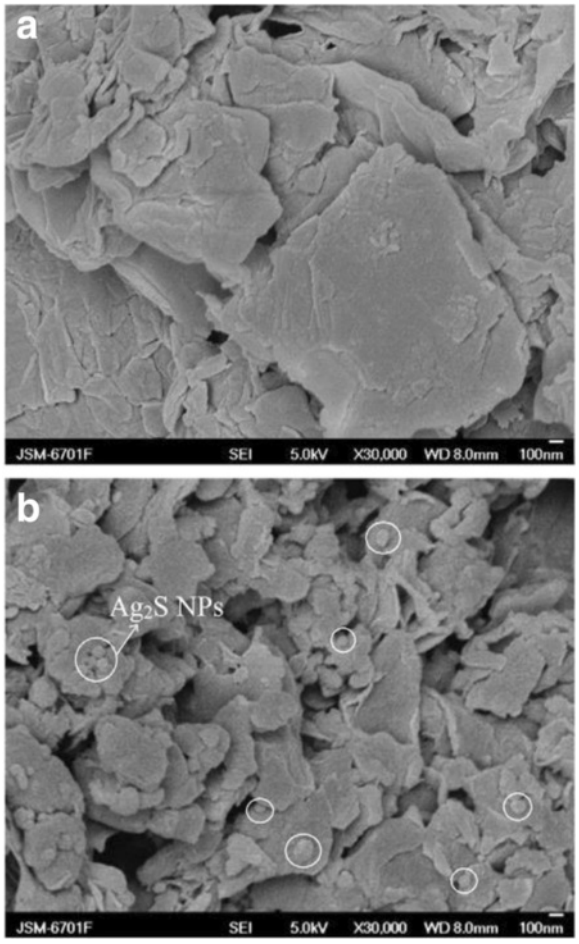

Fig. 26 SEM images of **a** the pristine graphene oxide and **b** Gs-Ag_2S composites [81]

limited its application [93]. Thus, increasing the precision of the Ag/Ag_2S electrode by surface micromotion can help the research work under extreme circumstances, such as hydrothermal vents [94, 95]. So, Ding et al. [96] have enhanced the sensitivity of the Ag/Ag_2S electrode by using direct current carrier power to electroplate silver nanoparticles on a silver wire. Three types of the Ag/Ag_2S electrode each had different physical structures under SEM (Fig. 28), which indicated that the different surfaces of these electrodes demonstrated that the preparation procedures affected the physical structures of the electrodes. Among all these electrodes, the direct current carrier electroplating electrode has the highest detection limit while the typical electrode has the lowest limit. From Table 2, we can see that the response time of the electrode prepared by direct

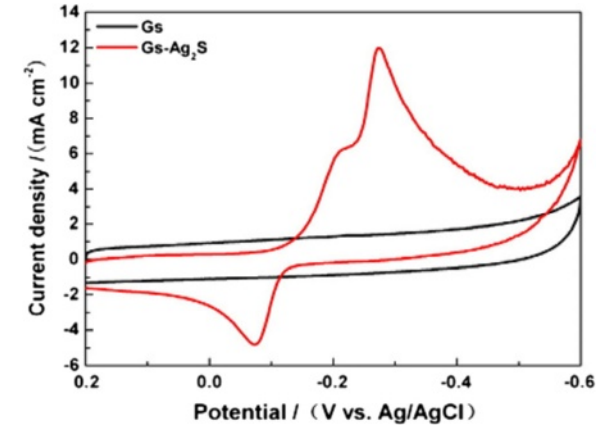

Fig. 27 CV curves of graphene and Gs-Ag_2S composites at 100 mV^{-1} in 1 M H_2SO_4 in potential range from −0.6 to 0.2 V [81]

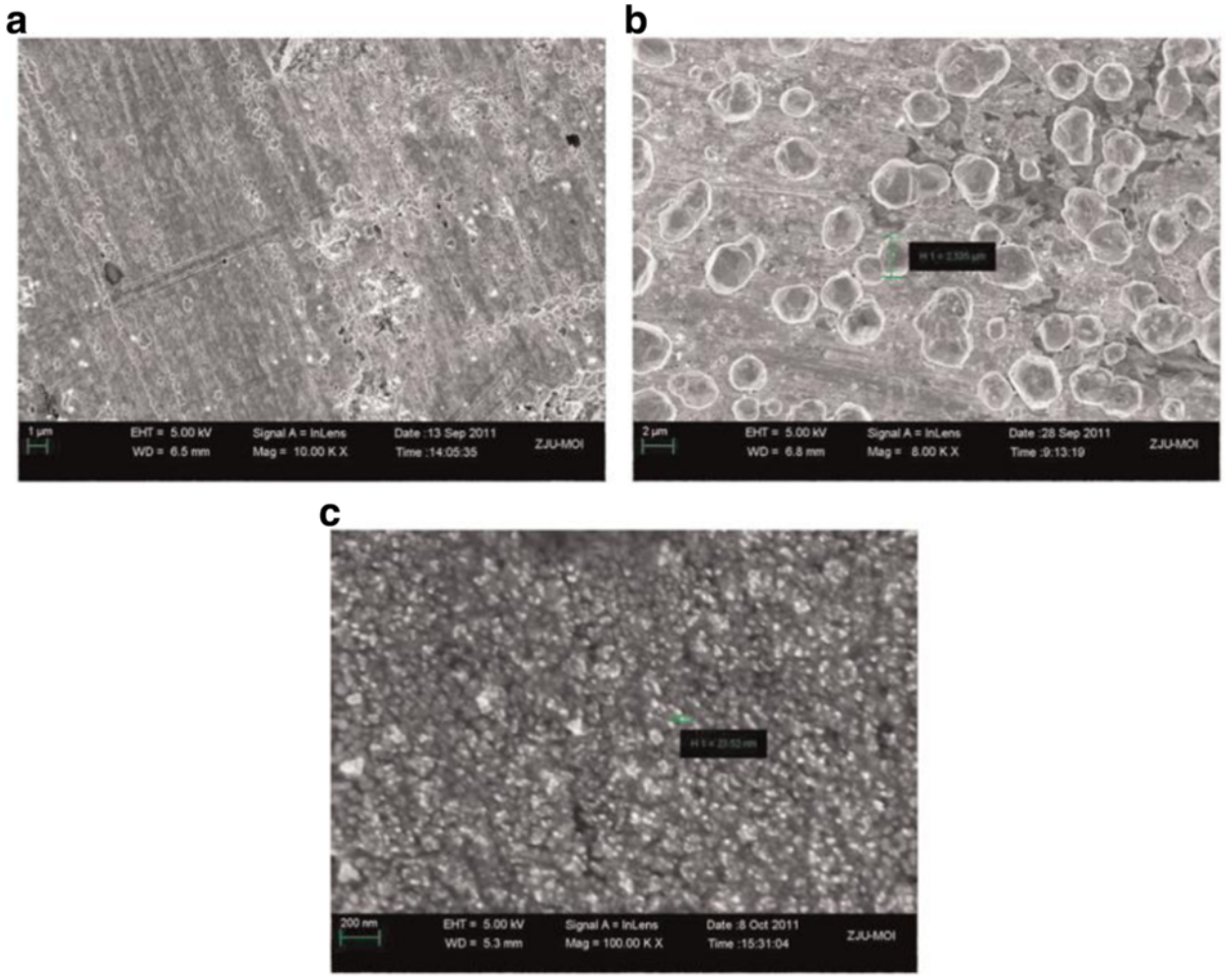

Fig. 28 SEM observation of the surface of **a** typical electrode, **b** direct current electroplating electrode, and **c** direct current carrier electroplating electrode [96]

current carrier electroplating for detecting a concentration of 10^{-7} mol L^{-1} S^{2-} was less than 60 s. And, the detection limits of the Ag/Ag_2S electrodes prepared by direct current electroplating and direct current carrier electroplating were improved to 1×10^{-5} and 1×10^{-7} mol L^{-1}, respectively. The RMSE (root mean square deviation) of the linear regression for the electrode using the direct current carrier electroplating method verified the accuracy and precision of this type of electrode (Fig. 29). In addition to the above mention, Ag_2S also has many other

Table 2 Correlation of EMF (mv) with-log[S^{2-}] for the types of electrode [96]

	slope	R2	*n*	RMSE	*p*
Typical	30.81	0.998	4	1.763	<0.001
DC electroplating	29.49	0.998	5	2.231	<0.0001
DC carrier electroplating	33.22	0.983	7	10.24	<0.0001

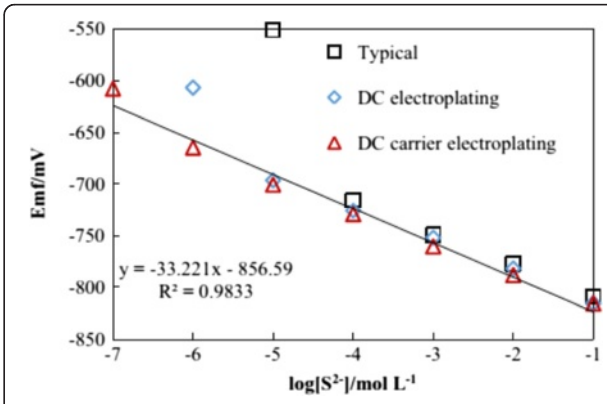

Fig. 29 Response curves of the three types of electrode. The linear correlation curve is generated using the direct current carrier electroplating method [96]

properties in applications, but it still needs people to explore it gradually.

Conclusions

Ag_2S, playing important functions in a number of optical, electrochemical, and biochemical process, has been regarded as a promising sensor and biological imaging agent in living creature. The preparation process and product of Ag_2S have many disadvantages in traditional preparation methods. For example, it usually needs high temperature, complicated processes, easy gather, and particle size bed control. Recently, considerable efforts have been made to optimize the productive process of Ag_2S and enhance properties and values of products. This work reviewed the progress in the development of Ag_2S nanomaterials in the field of synthesis and application. Different forms of Ag_2S nanostructures have been synthesized such as rod-shaped, leaf-shaped, and cubic. Ag_2S nanostructure obtained by bionic technology and precursor of decomposition were prepared successfully. Meanwhile, it has been applied to many fields successfully, such as optical, electrical, and biology, and it is expected to use in other fields. In fact, there are still limitations for their practical use in photoelectric and medical fields because it often requires complex preparation process, and the yield is very low. In most cases, Ag_2S nanoparticles are very prone to gather, which will greatly reduce its optical properties. Therefore, it is often necessary to composite with other materials to achieve a good effect. Although, there are so many challenges, the advances in nanoscience and nanotechnology of Ag_2S still promise a better future for kinds of industries.

Competing Interests

The authors declare that they have no competing interests.

Authors' Contributions

CC researched the existing literatures and wrote the manuscript. XL developed the concept and designed the manuscript. JL developed the concept. All the authors read and approved the final manuscript.

Acknowledgements

This work was supported by the Specialized Research Fund for the Doctoral Program of the Higher of Education (No. 20123706120003), Shandong Province Natural Science Fund of China (No. ZR2014EMQ002).

Received: 26 June 2015 Accepted: 16 October 2015
Published online: 02 November 2015

References

1. Jun HK, Gareem MA, Arof AK, Sust R (2013) Quantum dot-sensitized solar cells-perspective and recent development: a review of Cd chalcogenide quantum dots as sensitizers. Energy Rev 22:148–167
2. Selinsky RS, Ding Q, Faber MS, Wright JC, Jin S (2013) Quantum dot nanoscale heterostructures for solar energy conversion. Chem Soc Rev 42:2963–2985
3. PanL LT, Liu X, Lu T, Zhu G, Sun Z, Sun CQ (2012) Metal-free photocatalytic degradation of 4-chlorophenol in water by mesoporous carbon nitride semiconductors. Catal Sci Technol 2:754–758
4. Zhao Z, Liu Z, Miyauchi M (2010) Tailored remote photochromic coloration of in situ synthesized CdS quantum dot loaded WO_3 films. Adv Funct Mater 20:4162–4167
5. Ezenwa IA, Okereke NA, Egwunyenga NJ (2012) Optical properties of chemical bath deposited Ag_2S thin films. Int J Sci Technol 2:101–106
6. Hwang I, Yong K (2013) Environmentally benign and efficient Ag_2S-ZnO nanowires as photoanodes for solar cells: comparison with CdS-ZnO nanowires. Chem Phys Chem 14:364–368
7. Jiang F, Tian Q, Tang M, Chen Z, Yang J, Hu J (2011) One-pot synthesis of large–scaled Janus Ag-Ag_2S nanoparticles and their photocatalytic properties. Cryst Eng Comm 13:7189–7193
8. Dlala H, Amlouk M, Belgacem S, Girard P, Barjon D (1998) Structural and optical properties of Ag2S thin films prepared by spray pyrolysis. Eurphys j-appl phys 2:13–16
9. Brelle MC, Zhang JZ (1998) Femtosecond study of photo-induced electron dynamics in AgI and core/shell structural AgI/Ag_2S colloidal nanoparticles. Chem J Phys 108:3119
10. Bruhwiler D, Leigener C, Glaus S, Calzaferri G (2002) Luminescent silver sulfide clusters. J Phys Chem B 106:3770
11. Hull S, Keen DA, Sioia DS, Madden PA, Wilson M (2002) The high-temperature superionic behaviour of Ag_2S. J Phys Conclens Matter 14:19
12. Kitova S, Eneva J, Panov A, Haefke H (1994) Infrared photography based on vapor-deposited silver sulfide thin films. Imaging J Sci Fechnol 38:484
13. Wang DS, Hao CH, Zhong W, Peng Q, Wang TH, Liao ZM, Yu DP, Li YD (2008) Ultralong single-crystalline Ag_2S nanowires: promising candidates for photoswitches and room-temperature oxygen sensors. Adv Mater 20:2628
14. Liu JC, Raveendran P, Shervani Z, Ikushima Y (2004) Synthesis of Ag_2S quantum dots in water-in-CO_2 microemulsions. Chem Commun 22:2582–3
15. Xiao JP, Xie Y, Tang R, Luo W (2002) Template-based synthesis of nanoscale Ag_2E (E = S,Se) dendrites. J Mater Chem 12:1148–51
16. Chen M, Xie Y, Chen HY, Qiao ZP, Qian YT (2001) Preparation and characterization of metal sulfides in ethylenediamine under ambient condition through a γ-irradiation route. J Colloid Interf Sci 237:47–53
17. Lim WP, Zhang ZH, Low HY, Chin WS (2004) Preparation of Ag_2S nanocrystals of predictable shape and size. Angew Chem Int Ed 43:5685–9
18. Buda C, Chen XB, Narayanan R, Sayed EI (2005) Chemistry and properties of nanocrystals of different shapes. Chem Rev 105:1025
19. Zhang WQ, Xu LQ, Tang KB, Li FQ, Qian WT (2005) Solvothermal synthesis of NiS 3D nanostructures. Eur J Inorg Chem 4:653–656
20. Liu QY, Guo F, Komarneni S (2004) Biomolecule-assisted synthesis of highly ordered snowflakelike structures of bismuth sulfide nanorods. J Am Chem Soc 126:54–55
21. Kuang D, Xu A, Fang Y, Liu H, Frommen C, Fenske D (2003) Surfactant-assisted growth of novel PbS dendritic nanostructures via facile hydrothermal process. Adv Mater 15:1747–1750
22. Chen XG, Wang X, Wang ZG, Yang XG, Qian YT (2005) Hierarchical growth and shape evolution of HgS dendrites. Cryst Growth Des 5:347–350
23. Zhao Y, Zhang DW, Shi WF (2007) A gamma-ray irradiation reduction route to prepare rod-like Ag_2S nanocrystallines at room temperature. Mater Lett 61:3232–3234
24. Yin YD, XuXG GXW, Lu Y, Zhang ZC (1999) Synthesis and characterization of ZnS colloidal particles via γ-radiation. Radiat Phys Chem 55:353–356
25. Chen AH, Wang HQ, Li XY (2005) One-step process to fabricate Ag-polypyrrole coaxial nanocables. Chem Commun 14:1863–1864
26. Chen MH, Gao L (2006) Synthesis of leaf-like Ag_2S nanosheets by hydrothermal method in water alcohol homogenous medium. Mater Lett 60:1059–1062
27. Xu CG, Zhang ZC, Ye Q (2004) A novel facile method to metal sulfide (metal = Cd, Ag, Hg) nanocrystallite. Mater Lett 58:1671–1676
28. Cheng B, Russell JM, Sheng W, Zhang L, Samulski ET (2004) Large-Scale, solution-phase growth of single-crystalline SnO2 nanorods. J Am Chem Soc 126:5972–5973
29. Wong EM, Bonevich JE, Searson PC (1998) Growth kinetics of nanocrystalline ZnO particles from colloidal suspensions. J Phys Chem B 102:7770–7775
30. Zhai HJ, Wang HS (2008) Ag_2S morphology controllable via simple template-free solution route. Mater Res Bull 43:2354–2360
31. Gou LF, Murphy CJ (2003) Solution-phase synthesis of Cu_2O nanocubes. Nano Lett 3:231–234
32. Lee SM, Jun Y, Cho SN, Cheon J (2002) Single-crystalline star-shaped nanocrystals and their evolution: programming the geometry of nano-building blocks. J Am Chem Soc 124:11244–11245

33. Seo WS, Shim JH, Oh SJ, Lee EK, Hur NH, Park JT (2005) Phase- and size-controlled synthesis of hexagonal and cubic CoO nanocrystals. J Am Chem Soc 127:6188–6189
34. Lim WP, Zhang ZH, Low HY, Chin WS (2004) Preparation of Ag_2S nanocrystals of predictable shape and size. Angew Chem Int Ed 42:5803–5807
35. Wang XB, Liu WM, Hao JC, Fu XG, Xu BS (2005) A simple large-scale synthesis of well-defined silver sulfide semiconductor nanoparticles with adjustable size. Chem Lett 43:1664–1665
36. Dong LH, Chu Y, Liu Y (2008) Synthesis of faceted and cubic Ag_2S nanocrystals in aqueous solution. J Colloid Interf Science 317:485–492
37. Sun YZ, Zhou BB (2010) Single-crystalline Ag_2S hollow nanohexagons and their assembly into ordered arrays. Mater Lett 64:1347–1349
38. Zhuang ZB, Peng Q, Zhang B, Li YD (2008) Controllable synthesis of Cu_2S nanocrystals and their assembly into superlattice. J Am Chem Soc 130:10428–3
39. Zhuang Z, Peng Q, Wang X, Li Y (2007) Tetrahedral colloidal crystals of Ag_2S nanocrystals. Angew Chem Int Ed 46:8174–8177
40. Chaudhuri RG, Paria S (2012) A novel method for the templated synthesis of Ag_2S hollow nanospheres in aqueous surfactant media. J Colloid Interf Science 369:117–122
41. Liu MY, Xu ZL, Li BN, Lin CM (2011) Synthesis of worm-like Ag_2S nanocrystals in W/O reverse microemulsion. Mater Lett 65:555–558
42. Brelle MC, Zhang JZ, Nguyen L, Mehra RK (1999) Synthesis and ultrafast study of cysteine- and glutathione-capped Ag_2S semiconductor colloidal nanoparticles. J Phys Chem A 103:10194–201
43. Ortega EV, Berk D (2006) Precipitation of silver powders in the presence of ethylenediamine tetraacetic acid. Ind Eng Chem Res 45:1863–1868
44. Lv LY, Wang H (2014) Ag_2S nanorice: hydrothermal synthesis and characterization study. Mater Lett 121:105–108
45. Yu C, Ming ML, Liu Z, Yu Y (2012) Synthesis of normal and flattened rhombic dodecahedral Ag2S particles. Cryst Eng Comm 14:3772
46. McGrath KM (2001) Probing material formation in the presence of organic and biological molecules. Adv Mater 13(12–13):989–992
47. Cai W, Shin DW, Chen K, Gheysens O, Cao Q, Wang SX (2006) Peptide-labeled near-infrared quantum dots for imaging tumor vasculature in living subjects. Nano Lett 6:669–676
48. Kong Y, Chen J, Gao F, Li W, Xu X, Pandoli O (2010) A multifunctional ribonuclease-A-conjugated CdTe quantum dot cluster nanosystem for synchronous cancer imaging and therapy. Small 6:2367–2373
49. Yarema M, Pichler S, Sytnyk M, Seyrkammer R, Lechner RT, Fritz-Popovski G (2011) Infrared emitting and photoconducting colloidal silver chalcogenide nanocrystal quantum dots from a silylamide-promoted synthesis. ACS Nano 5:3758–3765
50. Du Y, Xu B, Fu T, Cai M, Li F, Zhang Y (2010) Near-infrared photoluminescent Ag2S quantum dots from a single source precursor. J Am Chem Soc 132:1470–1471
51. Chen J, Zhang T, Feng LL (2013) Synthesis of ribonuclease-A conjugate Ag_2S quantum dots clusters via biomimetic route. Mater Lett 96:224–227
52. Siva C, Chandrasekaran Nivedhini I (2014) L-cysteine assisted formation of mesh like Ag_2S and Ag_3AuS_2 nanocrystals through hydrogen bonds. MaterLett 134:56–59
53. Koneswaran M, Narayanaswamy R (2009) L-cysteine-capped ZnS quantum dots based fluorescence sensor for Cu^{2+} ion. Sens Actuator B Chem 139:104–9
54. de la Rica R, Velders AH (2011) Biomimetic crystallization of Ag_2S nanoclusters in nanopore assemblies. JAm Chem Soc 133:2875–2877
55. Brennan JG, Siegrist T, Carroll PJ, Stuczynski SM, Brus LE, Steigerwald ML. The preparation of large semiconductor clusters via the pyrolysis of a molecular precursor. J. Am. Chem. Soc. 1989:111;4141-4143.
56. Fan D, Afzaal M, O'Brien P (2007) Using coordination chemistry to develop new route to semiconductor and other materials. Coord Chem Rev 251:1878–1888
57. Esteves ACC, Trindade T (2002) Synthesis studies on II/VI semiconductor quantum dots. Curr Opin Solid State Mater Sci 6:347–353
58. Tang Q, Yoon SK, Yang HJ (2006) Selective degradation of chemical bonds: from single source molecular precursors to metallic Ag and semiconducting Ag_2S nanocrystals via instant thermal activation. Langmuir 22:2802–2805
59. Wang TX, Xiao H, Zhang YC (2008) Simple solid state synthesis of Ag_2S crystallites using a single source molecular precursor. Mater Lett 62:3736–3738
60. Zhang CL, Zhang SM, Yu LG, Zhang ZJ (2012) Size-Controlled synthesis of monodisperse Ag_2S nanoparticles by a solventless thermolytic method. Mater Lett 85:77–80
61. Hou XM, Zhang XL, Yang W, Liu Y (2012) Synthesis of SERS active Ag_2S nanocrystals using oleylamine as solvent reducing agent and stabilizer. Mater Res Bull 47:2579–2583
62. Shakouri-Arani M, Salavati-Niasari M (2014) Structural and spectroscopic characterization of prepared Ag_2S nanoparticles with a novel sulfuring agent. Mol Biomol Spectrosc 133:463–471
63. Wehrenberg BL, Wang C, Guyot-Sionnest P (2002) Interband and intraband optical studies of PbSe colloidal quantum dots. J Phys Chem B 106:10634–10640
64. Bakueva L, Gorelikov I, Musikhin S, Zhao XS, Sargent EH, Kumacheva E (2004) PbS quantum dots with stable efficient luminescence in the near-IR spectral range. Adv Mater 16:926–929
65. Harrison MT, Kershaw SV, Burt MG, Eychmuller A, Weller H, Rogac AL (2000) Wet chemical synthesis and spectroscopic study of CdHgTe nanocrystals with strong near-infrared luminescence. Mater Sci Eng B 69:355–360
66. Zrazhevskiy P, Senawb M, Gao X (2010) Designing multifunctional quantum dots for bioimaging, detection, and drug delivery. Chem Soc Rev 39:4326–4354
67. O'Connell MJ, Bachilo SM, Huffman CB, Moore VC, Strano MS, Haroz EH, Rialon KL, Boul PJ, Noon WH, Kittrell C (2002) Band gap fluorescence from individual single-walled carbon nanotubes. Science 297:593–596
68. Crochet J, Clemens M, Hertel T (2007) Quantum yield heterogeneities of aqueous single-wall carbon nanotube suspensions. J Am Chem Soc 129:8058–8059
69. Zhang Y, Hong GS, Zhang YJ (2012) Ag_2S quantum dot: a bright and biocompatible fluorescent nanoprobe in the second near-infrared window. ACS Nano 6(5):3659–3702
70. Jiang P, Zhu CN, Zhang ZL (2012) Water-soluble Ag_2S quantum dots for near-infrared fluorescence imaging in vivo. Biomaterials 33:5130–5135
71. Zhou XD, Shi HQ, Huang DM, Jia SM (2008) Room temperature synthesis and electrochemical application of imidazoline surfactant-modified Ag_2S nanocrystals. Mater Lett 62:2407–2410
72. Sohrabnezhad S, Pourahmad A (2010) Comparison absorption of new methylene blue dye in zeolite and nanocrystal zeolite. Desalination 256:84–89
73. Pourahmad A, Pourahmad A, Sohrabnezhad S, Rakhshaee R (2011) Ternary metal sulphide nanocrystals in MCM-41 nanoparticles matrix: preparation and properties. Micro Nano Lett 6:918–921
74. Aazam ES (2014) Photocatalytic oxidation of methylene blue dye under visible light by Ni doped Ag_2S nanoparticles. J Ind Eng Chem 20:4033–4038
75. Pourahmad A (2012) Ag_2S nanoparticle encapsulated in mesoporous material nanoparticles and its application for photocatalytic degradation of dye in aqueous solution. Superlattices and Microst 52:276–287
76. Robert D (2007) Photosensitization of TiO_2 by M_xO_y and M_xS_y nanoparticles for heterogeneous photocatalysis applications. Catal Today 122:20–26
77. Kim JC, Choi J, Lee YB, Hong JH, Lee JI, Yang JW, Lee WI, Hur NH. Enhanced photocatalytic activity in composites of TiO_2 nanotubes and CdS nanoparticles. Chem. Commun. 2006, 5024–5026. Epub 2006 Oct 27.
78. Puddu V, Mokaya R, Puma GL. Novel one step hydrothermal synthesis of TiO_2/WO_3 nanocomposites with enhanced photocatalytic activity.Chem. Commun. 2007, 4749–4751. Epub 2007 Sep 7.
79. Neves MC, Nogueira JMF, Trindade T, Mendonca MH (2009) Photosensitization of TiO_2 by Ag_2S and its catalytic activity on phenol photodegradation. J Photochem Photobiol A Chem 204:168–173
80. Shen SH, Guo LJ, Chen XB, Ren F (2010) Effect of Ag_2S on solar-driven photocatalytic hydrogen evolution of nanostructured CdS. Int J Hydrogen Energy 35:7110–7115
81. Mo ZL, Liu PE, Gou RB, Deng ZP (2012) Graphene Sheets/Ag_2S nanocomposites: synthesis and their application in supercapacitor materials. Mater Lett 68:416–418
82. Marti A, Araujo GL (1996) Limiting efficiencies for photovoltaic energy conversion in multigap systems. Sol Enrgy Mater Sol Cells 43:203
83. Auttasit T, Wu KL, Tung HY (2010) Ag_2S quantum dot-sensitized solar cells. Electrochem Commun 12:1158–1160
84. Karbmzadeh R, Aleali H, Mansour N (2011) Thermal nonlinear refraction properties of Ag2S semiconductor nanocrystals with its application as a low power optical limiter. Opt Commun 284:2370–2375
85. Xu MY, Niu HL, Huang JJ, Song JM, Mao CG, Zhang SY, Zhu CF, Chen CL (2015) Facile synthesis of graphene-like Co_3S_4 nanosheet/Ag_2S nanocomposite with enhanced performance in visible light photocatalysis. Appl Surf Sci 351:374–381
86. Li ZH, Shen J, Wang JQ, Wang DJ, Huang YJ, Zou J (2012) Single crystal titanate–zirconate nanoleaf: synthesis, growth mechanism and enhanced photocatalytic hydrogen evolution properties. Cryst Eng Comm 14:1874–1880

87. Sun YF, Sun ZH, Gao S, Cheng H, Liu QH, Lei FC, Wei SQ, Xie Y (2014) All-surface-atomic-metal chalcogenide sheets for high-efficiency visible light photoelectrochemical water splitting. Adv Energy Mater 4:1300611
88. Gubicza A, Csontos M, Halbritter A, Mihaly G (2015) Non-exponential resistive switching in Ag_2S memristors: a key to nanometer-scale non-volatile memory devices. Nanoscale 7:3493
89. Nasrallah TB, Dlala H, Amlouk M, Belgacem B (2005) Some physical investigations on Ag_2S thin films prepared by sequential thermal evaporation. Synth Met 151:225–230
90. Karashanova D, Nihtianova D, Starbov K (2004) Crystalline structure and phase composition of epitaxially grown Ag_2S thin films. Solid State Ionics 171:269–275
91. Hamilton JF (1988) The silver halide photographic process. Adv Phys 37:359–441
92. Karashanova D, Starbov N (2006) Surface assisted electric transport in Ag_2S thin films. Appl Surf Sci 252:3011–3022
93. Kuhl M, Steuckart C, Eickert G, Jeroschewski P (1998) A H_2S microsensor for profiling biofilms and sediments: application in an acidic lake sediment. Aquat Microb Ecol 15:201–209
94. Ding K, Seyfried WE, Tivey MK, Bradley AM (2001) In situ measurement of dissolved H_2 and H_2S in high temperature hydrothermal vent fluids at the Main Endeavour Field, Juan de Fuca Ridge. Earth Planet Sci Lelt 186:417–425
95. Zhang RH, Zhang XT, Hu SM (2013) Novel sensor based on Ag/Ag_2S electrode for in situ measurement of dissolved H_2S in high temperature and pressure fluids. Sens Actuators B Chem 177:163–171
96. Ding Q, Pan YW, Huang YF. The optimization of Ag/Ag_2S electrode using carrier electroplating of nano silver particles and its preliminary application to offshore Kueishan Tao, Taiwan. Continental Shelf Research. 2015, 25